Sediment availability on burned hillslopes

Article *in* Journal of Geophysical Research Atmospheres · December 2013

DOI: 10.1002/jgrf.20152

6 authors, including:

Petter Nyman
University of Melbourne
41 PUBLICATIONS **485** CITATIONS
SEE PROFILE

Gary James Sheridan
University of Melbourne
98 PUBLICATIONS **1,327** CITATIONS
SEE PROFILE

Hugh G. Smith
University of Liverpool
73 PUBLICATIONS **979** CITATIONS
SEE PROFILE

Patrick NJ Lane
University of Melbourne
84 PUBLICATIONS **1,373** CITATIONS
SEE PROFILE

Sediment availability on burned hillslopes

Petter Nyman,[1,2,3] Gary J. Sheridan,[1,2,3] John A. Moody,[4] Hugh G. Smith,[5] Philip J. Noske,[1] and Patrick N. J. Lane[1,2]

Received 4 November 2012; revised 21 September 2013; accepted 24 September 2013.

[1] Erodibility describes the inherent resistance of soil to erosion. Hillslope erosion models typically consider erodibility to be constant with depth. This may not be the case after wildfire because erodibility is partly determined by the availability of noncohesive soil and ash at the surface. This study quantifies erodibility of burned soils using methods that explicitly capture variations in soil properties with depth. Flume experiments on intact cores from three sites in western United States showed that erodibility of fire-affected soil was highest at the soil surface and declined exponentially within the top 20 mm of the soil profile, with root density and soil depth accounting for 62% of the variation. Variation in erodibility with depth resulted in transient sediment flux during erosion experiments on bounded field plots. Material that contributed to transient flux was conceptualized as a layer of noncohesive material of variable depth (d_{nc}). This depth was related to shear strength measurements and sampled spatially to obtain the probability distribution of noncohesive material as a function of depth below the surface. After wildfire in southeast Australia, the initial d_{nc} ranged from 7.5 to 9.1 mm, which equated to 97–117 Mg ha^{-1} of noncohesive material. The depth decreased exponentially with time since wildfire to 0.4 mm (or < 5 Mg ha^{-1}) after 3 years of recovery. The results are organized into a framework for modeling fire effects on erodibility as a function of the production and depletion of the noncohesive layer overlying a cohesive layer.

Citation: Nyman, P., G. J. Sheridan, J. A. Moody, H. G. Smith, P. J. Noske, and P. N. J. Lane (2013), Sediment availability on burned hillslopes, *J. Geophys. Res. Earth Surf.*, *118*, doi:10.1002/jgrf.20152.

1. Introduction

[2] Erodibility describes the inherent resistance of soil to erosion [*Bryan*, 2000]. It is a concept used to quantify the ease at which soil is detached by water and can be combined with measures of soil volume to determine sediment availability. Erodibility is determined by resistive forces in the soil such as friction, cohesion, and adhesion, which vary in space and time depending on the biological, physical, and geochemical factors that contribute to particle bonds, aggregation, and the formation of a structured matrix [*Bryan*, 2000; *Grabowski et al.*, 2011; *Gyssels et al.*, 2005; *Jenny*, 1994; *Kemper et al.*, 1987; *Tisdall and Oades*, 1982]. Erodibility is an empirical parameter derived from experiments. It is a measure of the amount of sediment detached under known flow conditions in laboratory flumes or on hillslope plots [*Elliot et al.*, 1989; *Govers et al.*, 1990; *Nachtergaele and Poesen*, 2002; *Robichaud et al.*, 2010; *Sheridan et al.*, 2007]. For example, in rill erosion, the erodibility is typically parameterized as a constant equal to the detached sediment per unit area divided by the applied shear stress or stream power (e.g., Water Erosion Prediction Project Model and European Soil Erosion Model) [*Laflen et al.*, 1997; *Morgan et al.*, 1998; *Nearing et al.*, 1989; *Moody et al.*, 2005].

[3] Wildfires can increase erodibility by (i) producing a new soil layer consisting of "ash" (defined in this paper to be a mixture of black soot, charcoal, and silt-sized mineral soil particles) [*Whicker et al.*, 2006; *Cerdà and Doerr*, 2008; *Gabet and Sternberg*, 2008; *Onda et al.*, 2008], and by (ii) heating and burning of the soil itself [*Moody et al.*, 2005; *Moody et al.*, 2013; *Robichaud et al.*, 2010; *Wilson*, 1999]. Heating and burning of the soil can cause an increase in erodibility because of impacts on binding agents such as roots, fungus, and organic compounds [*DeBano et al.*, 2005; *Giovannini and Lucchesi*, 1983; *Hart et al.*, 2005; *Hungerford et al.*, 1991; *Mataix-Solera et al.*, 2011; *Moody et al.*, 2005; *Neary et al.*, 1999]. Aggregate stability of the soil can be destroyed, and the near-surface root hairs are typically charred or consumed, resulting in a layer of unstructured and noncohesive soil containing highly erodible particles and aggregates [*Blake et al.*, 2007; *Gould*, 1998; *Mataix-Solera et al.*, 2011; *Parsons et al.*, 2010]. A layer of noncohesive ash and soil is an important

[1]Melbourne School of Land and Environment, University of Melbourne, Parkville, Victoria, Australia.
[2]Bushfire Cooperative Research Centre, East Melbourne, Victoria, Australia.
[3]eWater Cooperative Research Centre, University of Melbourne, Parkville, Victoria, Australia.
[4]U.S. Geological Survey, Boulder, Colorado, USA.
[5]School of Environmental Sciences, University of Liverpool, Liverpool, UK.

Corresponding author: P. Nyman, Department of Forest and Ecosystem Science, Melbourne School of Land and Environment, University of Melbourne, 221 Bouverie St, Parkville, Vic 3010, Australia. (nymanp@unimelb.edu.au)

2169-9003/13/10.1002/jgrf.20152

feature of burned hillslopes, which contributes to the increase in sediment fluxes and debris flow processes after wildfire [*Cannon et al.*, 2001; *Cerda and Lasanta*, 2005; *Gabet*, 2003; *Gabet and Bookter*, 2011; *Moody et al.*, 2008; *Nyman et al.*, 2011; *Smith et al.*, 2011; *Wells*, 1987]. The production and depletion of this noncohesive layer as a result of wildfire is poorly understood, and the effect on sediment availability has not been represented explicitly in erosion models.

[4] Impacts of a wildfire on soil properties are usually restricted to near-surface soils. Heat transfer during wildfires rarely extends more than 0.05 m into the soil profile, and charring is usually confined to the top 0.02 m of the soil [*DeBano et al.*, 2005; *Hungerford et al.*, 1991; *Parsons et al.*, 2010]. This means that erosion properties can exhibit strong variations with depth below the soil surface [e.g., *Cerdà and Doerr*, 2008; *DeBano et al.*, 2005; *Wells*, 1987]. Variations in soil erosion properties with depth are problematic when measuring erodibility in field experiments because sediment availability is changing while the soil is eroding [*Al-Hamdan et al.*, 2012; *Moffet et al.*, 2007; *Robichaud et al.*, 2010; *Sheridan et al.*, 2007]. This issue of changing sediment availability while the soil is eroding has been observed on road surfaces and soils subject to other types of disturbance [*Foltz et al.*, 2008; *Megahan*, 1974; *Ziegler et al.*, 2000].

[5] A temporally-averaged erodibility constant calculated from overland flow experiments fails to capture the time varying properties of erodibility. This is especially true during the initial flux of noncohesive sediment [*Wagenbrenner et al.*, 2010; *Ziegler et al.*, 2000], which can account for a large proportion of the sediment that is generated from burned hillslopes [*Cannon et al.*, 2001; *Cerda and Lasanta*, 2005; *Lane et al.*, 2011; *Nyman et al.*, 2011; *Sheridan et al.*, 2011; *Smith et al.*, 2012]. Ignoring the initial flux may produce a measure of erodibility which is insensitive to the effect of varying levels of disturbance. High-severity wildfires, for instance, can produce a heat pulse that penetrates deeper into the soil than low-severity wildfires [*Doerr et al.*, 2006; *Neary et al.*, 1999]. Hence, increased burn severity may increase the depth of charring (temperature >350°C) [*Hungerford et al.*, 1991] and increase the corresponding depth of the noncohesive layer. Millimeter-scale variation in the depth of the noncohesive layer can (depending on bulk density) translate to large differences in the initial mass of available material.

[6] The aim of the studies described in this paper was to develop a new framework for explicitly representing spatial and temporal changes in sediment availability as a result of wildfire. Three hypotheses were the following:

[7] 1. erodibility of fire-affected soils varies with root density and the depth below the soil surface;

[8] 2. sediment availability is transient (i.e. nonsteady) such that the sediment flux is initially high and decreases with time to a steady state; and

[9] 3. variation in the depth of noncohesive material is a measure of change in sediment availability.

[10] These hypotheses were formulated to help develop a stronger link between sediment availability on hillslopes and measures of fire severity, soil heating, and sediment depletion.

2. Methods

2.1. Overview

[11] The hypotheses were tested with data from three experiments. The specific objectives of these experiments were (1) to measure detachment rates as a function of depth in controlled laboratory conditions and to evaluate the effect of roots and soil physical properties, (2) to evaluate the temporal changes in sediment availability in the field by simulating overland flow in bounded erosion plots, and (3) to link spatial and temporal variations in soil shear strength to the depth of noncohesive layer on hillslopes that were recovering from wildfire.

[12] The first experiment was carried out on soil cores collected in coniferous forests (Colorado) and chaparral shrub (California) in western United States. The two other experiments were carried out in dry eucalypt forests (southeast Australia). Sites in western United States and southeast Australia were all burned by wildfire but represent contrasting vegetation communities and climatic settings. Experiments in the two regions had different specific objectives, but the outcomes are linked in terms of the conceptual representation of postwildfire erosion on hillslopes. The paper sets out to test hypotheses regarding erosion properties of burned soils in general, and including sites from different fire-prone regions provide greater scope for generalizing the patterns that emerge from the data.

2.2. Effects of Roots and Soil Properties on Variations in Erodibility With Depth

[13] Erodibility as a function of depth in fire-affected soil cores was quantified in a tilting flume. The data were analyzed with respect to soil properties such as root density and clay content, which have been shown to promote cohesiveness and resistance to erosion by overland flow [*Gyssels et al.*, 2005; *Knapen et al.*, 2007; *Waldron and Dakessian*, 1981]. The tilting flume experiments are described in detail by *Moody and Nyman* [2013] in a report containing raw data on the intrinsic root and soil properties, and on detachment rates at different depths. In the present paper, data from this report are used to calculate erodibility parameters and to determine the effects of intrinsic soil and root properties on erodibility. Density of roots near the soil surface was of particular interest because this property is sensitive to the effects of wildfire [*Parsons et al.*, 2010] and may play an important role in controlling sediment availability [*Gould*, 1998].

[14] Intact soil cores were collected from areas that had been recently burned and which had different geology, soil, and vegetation. One area was burned by the 2010 Fourmile Canyon fire in the Front Range of the Rocky Mountains near Boulder, Colorado [*Ebel et al.* 2012], and the other area was burned by the 2010 Pozo fire in the La Panza Mountains, which are part of the central California Coastal Mountains near San Luis Obispo, California [*Moody and Nyman*, 2013]. The 2010 Fourmile Canyon fire (~2500 ha; Figure 1a, Table 1) burned through primarily ponderosa pine (*Pinus pondersosa*) and Rocky Mountain juniper (*Juniperus scopulorum*) on south-facing (xeric) slopes and primarily Douglas fir (*Pseudotsuga menziesii* subspecies *glauca*) and limber pine (*Pinus flexilis*) on north-facing (mesic) slopes. Soils on the south-facing site are stony and gravelly

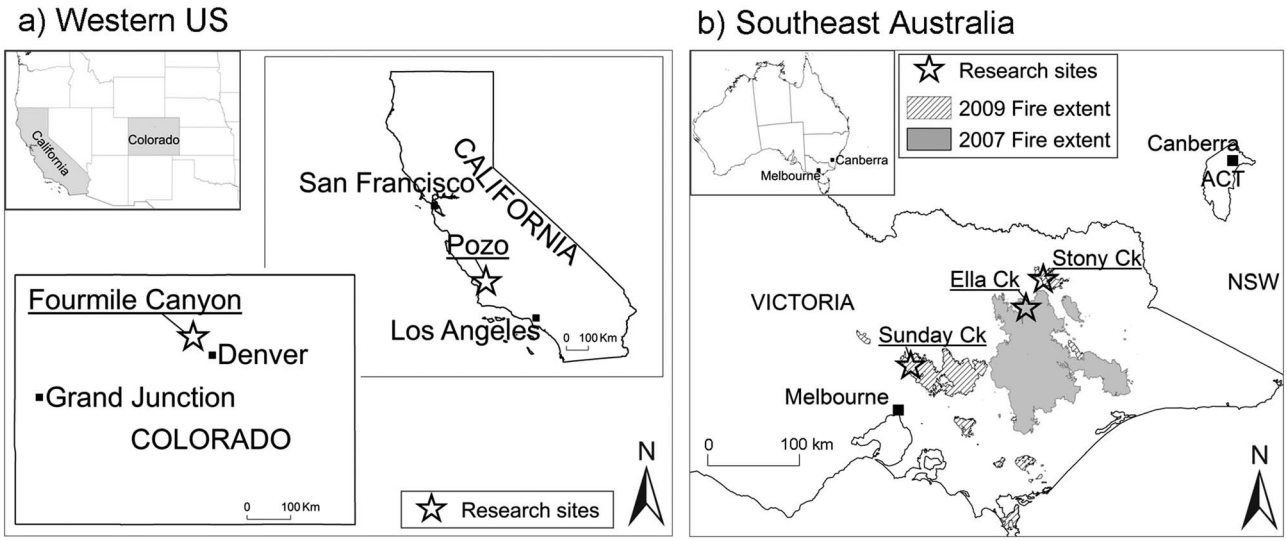

Figure 1. Map showing the location of research sites in (a) western United States (Fourmile Canyon in Colorado and Pozo in California) and (b) southeast Australia (Sunday Creek, Stony Creek, and Ella Creek in Victoria).

sandy loams, while soils on the north-facing site are primarily coarse to fine gravelly sandy loams. The 2010 Pozo fire (~500 ha; Figure 1a, Table 1) burned through chaparral vegetation consisting of scattered blue oak (*Quercus douglasii*), manzanita (*Arctostaphylos* sp.), chamise (*Adenostoma* sp.), and white sage (*Salvia apiana*). Soils are fine clay loams derived from bedrock consisting of marine sedimentary rocks.

2.2.1. Soil Samples

[15] Replicate intact soil cores for measurements of erodibility and soil samples for measurement of soil properties were collected at each site. Within the Fourmile Canyon fire, these were collected at three locations at elevations between 2350 and 2450 m on a north- and on a south-facing site with hillslope lengths on the order of 200–400 m and slopes of 20–30°. At Pozo, they were collected at three locations at elevations between 500 and 580 m on short (50–100 m), steep (20–40°) south-facing hillslopes. An unburned location was sampled at sites in comparable catchments. Five intact soil cores (7.5 cm long, 4.7 cm diameter) were collected at each of the three locations and used in the flume experiments to measure detachment rates as a function of depth. Six soil cores (10 cm long, 4.7 cm diameter core) were collected at each location and subsampled at five depth intervals (0–0.01,

Table 1. List of Research Sites Used in Different Components of the Study

Site	Aspect	Soil Burn Severity[a]	Annual Rainfall (mm)	Forest Type and Dominant Vegetation	Geology	Soil Texture/Bulk Density, (0–5 cm) $(kg\,m^{-3}) \times 10^3$
			Laboratory Study: *Western United States*			
Fourmile Canyon 40°02′4″N 120°24.4″N	South (xeric)	Moderate severity Sep 2010	500–600	Coniferous, Ponderosa Pine (*Pinus pondersosa*)	Granite	Stony and gravelly sandy loams BD = 1.34
Fourmile Canyon 40°02′5″N 105°24′1″W	North (mesic)	Moderate to high severity Sep 2010	500–600	Coniferous, Douglas Fir (*Pseudotsuga menziesii* subspecies *glauca*)	Granodiorite	Coarse to fine gravelly sandy loams BD = 1.21
Pozo 35°19′4″N 120°19′3″W	South (xeric)	Moderate to high severity Aug. 2010	500–600	Chaparal, Manzanita (*Arctostaphylos* sp.), Chamise (*Adenostoma* sp.),	Marine sedimentary	Fine clay loam BD = 1.27
			Field Study: *Southeast Australia*			
Ella Creek, 36°47′1″S 146°34′5″E	North (xeric)	Moderate to high severity Dec 2006	1200–1400	Dry eucalypt, Broad-leaved peppermint *(Eucalyptus radiata)* Narrow-leaved peppermint (*Eucalyptus dives*)	Shale, Marine Sedimentary	Stony and gravelly clay loam *BD* = 0.94
Sunday Creek 37°21′3″S 145°07′4″E	North (xeric)	High severity Feb 2009	1000–1200	Dry eucalypt, Broad-leaved peppermint (*Eucalyptus radiata*)	Siltstone, Marine Sedimentary	Stony and gravelly clay loam BD = 1.22
Stony Creek 36°30′2″S 146°48′2″E	North-west (xeric)	High severity Feb 2009	1000–1100	Dry eucalypt, Broad-leaved peppermint (*Eucaluptus radiata*)	Phyllite and Gneiss Metamorphic	Gravelly clay loam BD = 1.27

[a]The soil burned severity assessed visually at each site based on the field guide for mapping soil burn severity [*Parsons et al*., 2010].

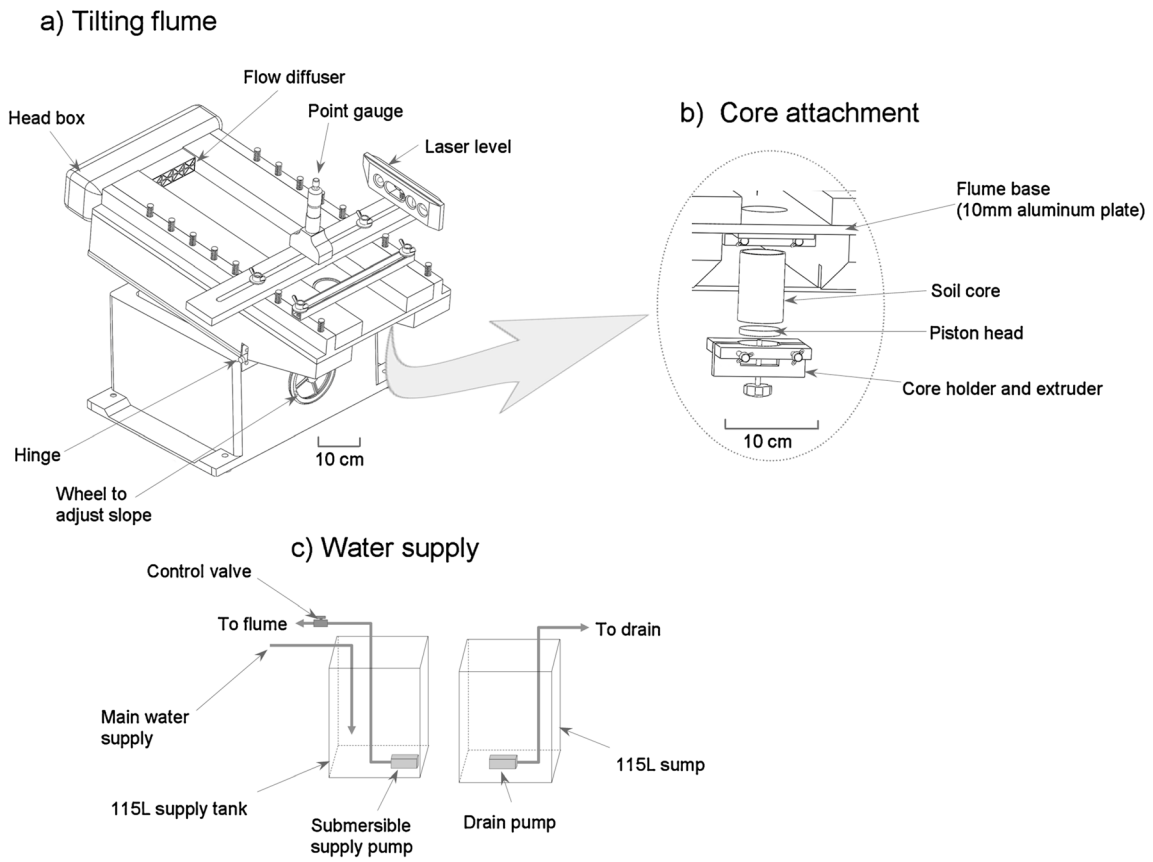

Figure 2. The components of the (a) tilting flume, (b) core attachment and extruding device, and the (c) water supply system. Figure modified from *Moody and Nyman* 2013.

0.01–0.03, 0.03–0.05, 0.05–0.075, 0.075–0.10 m). Three of these subsampled cores were used to measure loss on ignition, LOI, (%), bulk density, BD, (kg m^{-3}), and particle-size distribution; and three were used to measure root density, RD, (kg m^{-3}), and root-length density, RLD, (m m^{-3}). These data on soil and root properties at different depths are given by *Moody and Nyman* [2013].

2.2.2. Detachment Rates

[16] Detachment rates were measured in shallow water, adjustable tilting flume [*Moody and Nyman*, 2013]. The flume (10 cm wide, 50 cm long, and maximum depth of 2.5 cm; Figure 2a) had a 5.1 cm diameter hole in the flume bed where the intact soil core was mounted underneath, together with a piston for extruding the sediment core (Figure 2b). Clear water was pumped from the supply tank through the head box of the flume, and the discharge, Q ($0.2–12.0 \times 10^{-4}$ m^3 s^{-1}), was manually controlled by an inline butterfly valve (Figure 2c). Water left the head box through a diffuser, flowed down the flume, across the soil core, and fell off the flume bed into a 115 L sump tank.

[17] The shear stress, τ_f (Pa), for uniform flow is a function of slope, S, and water depth, h_w (m)

$$\tau_f = \rho g h_w S \tag{1}$$

where ρ is density of water (1000 kg m^{-3}), and g is acceleration of gravity (9.8 m s^{-2}). Water depth was measured using a point gage mounted 7.5 cm upstream from the center of the core. Accuracy of the point gauge was 0.005 cm, but the fluctuating water surface over the cores reduced the precision of the depth measurements to 0.05 cm. During calibration, the depth measurements at a second point gauge 7.5 cm downstream from the center of the core indicated that flow was accelerating. Two terms were therefore added to equation (1) to represent the shear stress caused by change in mean velocity and change in pressure between two points [*Julien*, 1998]. If h_{w1} (m), h_{w2} (m), $\overline{u}_1$ (m s^{-1}), and $\overline{u}_2$ (m s^{-1}) are the water depths and mean cross-sectional velocities at point gauge 1 and 2 separated by a distance, d (m), then the nonuniform shear stress, τ_{fn} (Pa), is given by

$$\tau_{fn} = \rho h_w [gS + ((\overline{u}_1 + \overline{u}_2)/2)(\overline{u}_1 - \overline{u}_2)/d + ((h_{w1} + h_{w2})/2)(h_{w1} - h_{w2})/d] \tag{2}$$

[18] Estimates of the four nonuniform shear stresses, τ_{fn} (2.2, 6.3, 14.4, and 42.1 Pa), used in the experiments were determined from measurements of depth and discharge using a smooth plug in place of the soil core (to eliminate the effects of soil roughness).

[19] Each individual core provided five measurements of the detachment rate, E (kg m^{-2} s^{-1}), for each value of τ_{fn} at five different soil depths, d_s (m). Each measurement was obtained from a unique depth in the soil core, which fell within a small depth interval around the target depth. Target soil depths, d_s (m), were 0.001 (surface), 0.005, 0.02, 0.04, and 0.06 m. For the first core, a value of τ_{fn} was selected and measurements were made at all values of d_s keeping τ_{fn} constant. A second core was then used for measurements for a different value of τ_{fn} at all values of d_s.

Thus, soil detachment was measured at all four values of τ_{fn} by using four of the five intact cores from one location (the fifth core was archived). Each burned site had three locations, which provided three replicate measurements of E for each value of τ_{fn}. The reader is referred to the report published by *Moody and Nyman* [2013] for details of the experiment procedure.

[20] A linear function was used to describe a general relation between detachment rate E and nonuniform shear stress (τ_{fn}) ($E = 0.0019\,\tau_{fn}^{1.00}$, $R^2 = 0.23$) [*Moody and Nyman*, 2013]. The proportionality constant in this relation is defined as the erodibility, k_d (s m^{-1}), of the soil [e.g., *Foster*, 1995; *Wagenbrenner et al.*, 2010]. Critical shear stress for initiating erosion was assumed to be negligible in these experiments because the critical shear stress for typical particles (0.063–1.0 mm) is 0.2–0.8 Pa [*Moody et al.*, 2005; *Wiberg and Smith*, 1987], which is smaller than the shear stress used in the experiments (2.2–42.1 Pa). Erodibility at each depth was then calculated as

$$k_d = \frac{E}{\tau_{fn}} \tag{3}$$

[21] All k_d values within each sampling location were ranked by the measurement depth, d_s, and averaged in groups of four. This produced a single erodibility value at each location corresponding to an average of four target depths.

2.2.3. Soil and Root Analyses

[22] Subsampled soil cores were used to determine soil and root properties as a function of depth. There were nine cores per site for soil analysis, nine cores for root analysis, and each core was subsampled at five depth intervals. Samples for soil analyses were dried at 105°C for 24 h, weighed to determine the total mass, and split into two parts: one part was used for particle-size analysis and one part was used for soil organic content analysis measured as the loss on ignition (LOI) at 500°C for 2 h [*Heiri et al.*, 2001]. Particle-size distribution was determined by using standard sieve methods [*Guy*, 1977]. Bulk density, BD, was computed from the total oven dry mass, the thickness (depth interval) of the sub-sample, and the diameter of the core.

[23] Samples for root analyses (root density (RD) and root-length density (RLD)) were first air dried, then weighed and poured gently onto a 2 mm sieve. Roots which were easily detected were collected before sieving in order to avoid unnecessary fragmentation. Sieved soil and roots were washed into a white enamel tray with a gridded base (5 cm grid squares) filled with water to an approximate depth of 1 cm, then systematically collected with tweezers at each grid under a 10× magnification [*De Baets et al.*, 2006]. In cases where roots were highly abundant and where there was little other floating material, the roots could be extracted using a suction pipette. This method was more time efficient, but was not suitable for samples with abundant organic material, which would contaminate the root sample and lead to bias in the root-mass measurements. Root mass was measured to nearest 0.001 g, after drying at 65°C for 48 h. Live and dead roots could not be distinguished. However, charred roots disintegrate when disturbed leaving behind a sooty residue. These could be distinguished and were not extracted. All other roots (length >1 mm, diameter <2 mm) were extracted. Root length was measured using the line intersect method [*Tennant*, 1975]. All intersections between roots and grid lines were counted for each individual sample from photographs. The line intersect method was validated for a subset of samples by estimating root length using manual length measurements, direct intersect counts, and counts from photographs [*Moody and Nyman*, 2013].

2.3. Temporal Changes in Sediment Availability

[24] Data on temporal changes in sediment availability were obtained from erosion plot experiments. These experiments simulated overland flow inside bounded plots to capture changes in the sediment flux with time, starting with the initial flux of easily eroded sediment and ending with the depletion of sediment on the plots. Experiments were performed on a hillslope in dry eucalypt forest in southeast Australia that was burned during the catastrophic Black Saturday wildfires in 2009 (Figure 1b, Table 1). Wildfires burned over 450,000 ha, mostly in a short period of time (~12 h) under exceedingly dry fuels and extreme fire weather [*Cruz et al.*, 2012]. The site was located near Sunday Creek Reservoir (~50 km north of Melbourne) in a catchment dominated by broad-leaved peppermint (*Eucaplytus radiata*) and consisting of stony and gravelly clay loam derived from marine sedimentary rocks. Three field plots (4 m long by 0.15 m wide) were installed on a planar, north-facing (xeric) slope close to a ridge top in an area where the burned soil was intact and appeared unaffected by overland flow. A discrete ash layer was not apparent, presumably because of compaction, mixing, wind, and interrill erosion prior to the experiments. Steel edging (1 m long segments) was carefully driven into the soil and stabilized using steel pegs inserted along the outer edge. Slope gradient, S, was determined for each plot as the average change in height across 1 m horizontal segments at the top, mid, and bottom section of the test area. Average slope gradient for the three plots were 0.36, 0.39, and 0.40.

[25] Erosion plot experiments were run as a sequence of successively increasing values of discharge. Water was pumped from a supply tank (2000 L) and delivered to a small reservoir at the top the plot where the discharge, Q (2, 5, 10, and 15×10^{-4} m^3 s^{-1}), was controlled manually by a ball valve and measured with a flow meter. At the bottom of the plot, water and sediment were diverted through a 100 cm long by 15 cm diameter pipe to a collection point where they were sampled in 0.5 L containers at six time intervals during each 60 s sampling period for each discharge. Sediment concentration samples for calculating the sediment flux, q_s (kg m^{-1} s^{-1}), were collected when the initial surge of water and sediment reached the collection point ($t = 0$ s), and then every 10–15 s afterward by sweeping the 0.5 L container through the flow three times. Sediment that was not diverted was continuously collected in a 20 L overflow bucket at the collection point. After 60 s, the samples contained very little sediment (relative to what was collected during the initial erosion), and the sediment flux was assumed to be at a steady state. Data from similar experiments in these type of systems indicate that after 60 s the sediment flux approaches a steady state with a relatively small decrease in erodibility from 2.2×10^{-4} to 1.8×10^{-4} s m^{-1} by adding 30 s to the measurement period [*Sheridan et al.*, 2007]. Sediment flux may have decreased a little more if the experiment was run for a longer period of time, but this decrease would be small

compared to the magnitude of change during the initial erosion and would have little impact on the overall mass of sediment produced from the plot. This study was primarily concerned with the material that eroded during the initial flux, so the 60 s was a reasonable trade-off between the logistical constraints of water availability in the supply tank and the data requirements.

[26] Flow depth, h_w, for each level of Q was measured to the nearest millimeter using a metal ruler at eight points along flow paths within the plot and used to calculate the shear stress, τ_f. Flow velocity, u_{dye} ($\mathrm{m\,s^{-1}}$), was measured three times for each discharge using a dye tracer that was injected at the top of the test area and timed until the dye front had reached the collection point at 4 m.

[27] Sediment flux per unit width, q_s ($\mathrm{kg\,m^{-1}\,s^{-1}}$), was calculated from the mass of sediment (collected in the 0.5 L containers) after drying in laboratory at 105°C. At the top of the plot, the width of the flow was equal the width of the plot. Within the plot, however, the width of the flow was spatially variable and changed depending on the discharge. Nonuniform flow within the plot was a result of flow paths which formed within the noncohesive material that mantled the underlying cohesive substrate. Sediment fluxes, q_s, and unit discharges, q_w ($\mathrm{m^2\,s^{-1}}$), were calculated based on the entire width of the plot (i.e., the entire surface available for erosion) rather than the actual width of the flow within the plot. Hence, the changes in q_s with time (t) and with increasing unit discharge, q_w, were interpreted as changes in sediment availability relative to the total mass of noncohesive material stored on the surface.

[28] A detachment rate, E ($\mathrm{kg\,m^{-2}\,s^{-1}}$), was calculated from q_s once the flux approached steady state ($45 < t < 60$ s) and is given for the erosion plots by equation (4)

$$E = \frac{q_s}{w} \tag{4}$$

where $w = Q/h_w\overline{u}$ is the flow width and $\overline{u}$ ($\mathrm{ms^{-1}}$) is the average flow velocity measured as $\overline{u} = \alpha u_{\mathrm{dye}}$. The coefficient, α, (a function of the surface velocity profile) was obtained at the highest discharge ($Q = 15 \times 10^{-4}\ \mathrm{m^3\,s^{-1}}$), when the flow was uniform across the plot ($w = 0.15$ m). Total sediment yield (in $\mathrm{kg\ m^{-2}}$) from the plot was estimated from the sum of sediment in 0.5 L containers and the 20 L overflow bucket. Sharpened erosion pins (15 cm long by 0.4 cm diameter) were inserted prior to the experiments in a line going downslope at eight points spaced at regular intervals inside the plot. The height of a reference point on each pin was measured before and after each experiment and used to calculate the average depth of erosion after the highest discharge had been applied.

[29] Particle-size distribution of eroded material was determined for individual 0.5 L containers collected from the flume. Each oven dried sample was gently disaggregated and placed in a nest of sieves to separate gravel ($2 < D \leq 16$ mm), coarse sand ($0.6 < D \leq 2$ mm), fine and medium sand ($0.063 < D \leq 0.6$ mm), and silt and clay ($D < 0.063$ mm). Measurements were then combined across each of the three replicate experiments based on the time intervals 0–1, 1–15, 16–35, and 36–55 s to produce an average particle-size distribution as a function of time. There was no discrete ash layer at Sunday Creek, and the contribution of ash to erosion was not distinguished from the contribution of the mineral soil. Density of soil and ash particles can be similar [*Cerdà and Doerr*, 2008; *Kinner and Moody*, 2008; *Gabet and Bookter*, 2011; *Moody and Ebel*, 2012], and the ash component often includes a mineral component that is incorporated by wind and water [e.g., *Whicker et al.*, 2006; *Onda et al.*, 2008; *Moody and Ebel*, 2013]. In the context of sediment transport during the erosion plot experiments, it is therefore reasonable to consider ash and the soil as part of a combined pool of available sediment. Distinguishing between soil and the vegetative ash would require analysis into the relative solubility of ash and soil as well as the chemical composition of the source material, something which was outside the scope of this paper.

2.3.1. Linking Sediment Availability to Soil Shear Strength

[30] Sediment flux in the erosion plot experiments was linked to measurements of soil shear strength. Soil shear strength, τ_v (kPa), was measured by using a shear vane (HM-504A Pocket Shear Vane Set; total range = 0–250 kPa; vane diameter = 5.1 cm) at 10 points along a transect on a noneroded section of soil adjacent to each of the three field erosion plots at Sunday Creek. The noncohesive surface material along the transect was intact and had not been affected by surface runoff. The shear vane measures the maximum internal resistance of a soil to a rotational movement of its particles and can be used to quantify soil erodibility [*Léonard and Richard*, 2004; *Rauws and Covers*, 1988]. Measurements were repeated at five depths (0, 0.01, 0.03, 0.06, and 0.09 m) at each sampling point by carefully excavating a small trench using the end of a metal ruler to expose an area for each new depth measurement. Vane blades were 0.005 m high, so the measurement was the average of a small 0.005 m depth interval and was plotted using the midpoint of the depth interval. Depth profiles of τ_v were used to obtain a τ_v threshold which corresponded with the transition from noncohesive to cohesive material. The distinction between noncohesive and cohesive material was made based on the depth at which sediment flux (from the adjacent erosion plots) transitioned from nonsteady to steady state.

2.4. Availability of Noncohesive Soils in Burned Headwaters

[31] An extensive survey of soil shear strength was carried out in order to capture the temporal changes in erosion properties of the soil during a 0–3 year postwildfire period. Surveys were carried out in headwater (zero order) catchments of Ella Creek, Sunday Creek, and Stony Creek in the eastern uplands of Victoria, southeast Australia (see Figure 1b and Table 1). Stony Creek and Sunday Creek were burned in February 2009, and measurements were made in September 2009 and March 2010, 0.5 and 1 year after the wildfire, respectively. Ella Creek was burned in January 2007, and measurements in September 2009 and March 2010 represent conditions 2.5 and 3 years after the wildfire. Inclusion of Ella Creek means that the measurements spanned a longer recovery window. Substituting space for time assumes that spatial and temporal variations are equivalent. Ella Creek was considered to be suitable in this respect given its similarities to Stony Creek and Sunday Creek in terms of soil, vegetation, and fire impact (Table 1).

Table 2. Correlations Between Soil Properties and Erodibility, k_d, at Different Depths[a]

Depth Interval (m)	Statistics	Bulk Density BD ($kg\,m^{-3}$)	Loss on Ignition LOI (%)	Root Density RD ($kg\,m^{-3}$)	Root-Length Density RLD ($m\,m^{-3}$)	Silt and Clay Content (%)
0–0.01	Pearson's r	−0.25	−0.37	**−0.58**	**−0.37**	0.12
	p value	0.167	0.84	**0.001**	**0.04**	0.52
0.01–0.03	Pearson's r	0.29	−0.5	−0.26	0.03	−0.42
	p value	0.37	0.87	0.42	0.93	0.17
0.03–0.05	Pearson's r	**0.54**	−0.46	−0.127	0.07	**−0.53**
	p value	**0.07**	0.13	0.97	0.82	**0.07**

[a]Significant correlations ($p < 0.1$) are in bold font.

[32] Each headwater catchment was sampled at three distances from the ridge top along three evenly spaced transects running perpendicular to the contours. Three replicate measurements were conducted at random points in a 2 m^2 quadrat at each sampling location (0, 40, and 80 m from the ridge top). At each point, the soil shear strength was measured at five depths using the same protocol as the measurements taken as part of the erosion plot experiments (see section 2.3.1). One headwater (three transects) was sampled at Ella Creek and Stony Creek, and two replicate headwaters (six transects) were measured at Sunday Creek. The aim of the first sampling campaign (September 2009) at Sunday Creek and Stony Creek was to characterize the properties of fire-affected material, which covered the soil immediately following the wildfire. Lower sections of the hillslopes at these sites had been affected by surface runoff in 6 months prior to when the measurements were obtained. The 2 m^2 quadrat was therefore positioned outside of the areas where surface runoff paths had obviously eroded the surface soil. Repeat measurements in March 2010 were made in quadrats placed on the opposite side of the sampling transect in order to avoid disturbance effects from the first sampling. Measurements within quadrats were sampled randomly from eroded and noneroded surfaces. Soil moisture was measured gravimetrically on soil samples collected at each sampling quadrat (composited by hillslope position) and at depth intervals that corresponded with the depth of shear vane measurements. Material collected from the two upper sampling depths (0–0.01 m) was analyzed for particle-size distribution, loss on ignition (LOI), and solubility.

[33] Soil shear strength declines with increasing soil moisture content, particularly when gravimetric moisture contents is less than 20% [*Chorley*, 1959; *Zimbone et al*., 1996]. The temporal variability in shear strength due to recovery could therefore only be analyzed once measurements were adjusted for the temporal variation caused by soil moisture. Relative moisture content (volumetric water content relative to porosity) in September 2009 and March 2010 in the two upper soil depths (0 and 0.01 m) was relatively low (33–29%) and did not differ between the two campaigns at any of the sites. For measurements at greater depths ($d_s \geq 0.03$ m), however, the relative moisture content in September 2009 (40–44%) was significantly higher ($p < 0.01$) than in March 2010 (30–36%) at all sites (t value = 16.8; d.f. = 52). A linear adjustment function ($\tau_{v\ \mathrm{March}} = 0.9\tau_{v\ \mathrm{Sept}} + 0.15$; $n = 9$; $R^2 = 0.97$) was obtained at all three sites for the measurements where $d_s \geq 0.03$ m. This adjustment function ensured that temporal trends in $\tau_v(d_s)$ for $d_s < 0.03$ m could be interpreted independently from effects of subsurface moisture fluctuations. The moisture fluctuations in subsurface soils and their effects on shear strength are noteworthy, however, because they may be important when modeling initiation of channels and subsequent entrainment processes [e.g., *McCoy et al*., 2012].

3. Results

3.1. Effects of Roots and Soil Properties on Variations in Erodibility With Depth

[34] The influence of soil properties, root density (RD), and root-length density (RLD) on erodibility was initially explored by simple correlations for each soil depth (Table 2). Root properties were found to be the most influential variable at the soil surface (0–0.01 m), whereas percent of silt and clay and the bulk density were the most influential at lower depths (0.03–0.05 m). Percent of silt and clay are also the soil variable which displayed the largest differences between sites at the lower depths [*Moody and Nyman*, 2013]. In the depth interval from 0.01 to 0.03 m, none of the variables were significantly correlated with erodibility, indicating that this is a transitional zone where no single variable emerged as the dominant predictor.

[35] This paper is concerned with the erodibility of soils that have been impacted by the wildfire, and therefore the remaining analysis is constrained to depths <0.02 m for three reasons. First, the erodibility within this zone deviated strongly from the relatively resistant subsurface soil (Figure 3); second, this is the depth range where heat impacts are most likely; and third, below this depth range, there is a shift in the influence of roots (see Table 2). Erodibility decreased exponentially with d_s between the soil surface and $d_s = 0.02$ m (Figure 3), and the relatively low value of k_d at 0.02 m was assumed to represent a constant erodibility below the noncohesive layer (i.e., $d_s > 0.02$ m). These constant erodibility values (at ~0.02 m depth) for Fourmile Canyon (FMC) North, FMC South, and Pozo, respectively, were 1.48, 2.03, and $1.72 \times 10^{-4}\,s\,m^{-1}$, with similar levels of variability for all sites (coefficient of variation, CV = 0.95–1.00). The average surface erodibility of four burned soil cores at FMC North ranged from 8.37 to $38.8 \times 10^{-4}\,s\,m^{-1}$. At FMC South, the corresponding values were 19.4–$122 \times 10^{-4}\,s\,m^{-1}$, and at Pozo, they ranged from 15.3 to $61.6 \times 10^{-4}\,s\,m^{-1}$. Unburned cores consistently displayed the lowest erodibility (0.7–$13.2 \times 10^{-4}\,s\,m^{-1}$) on the soil surface, although at Pozo the unburned surface erodibility was high ($13.2 \times 10^{-4}\,s\,m^{-1}$) (Figure 3c).

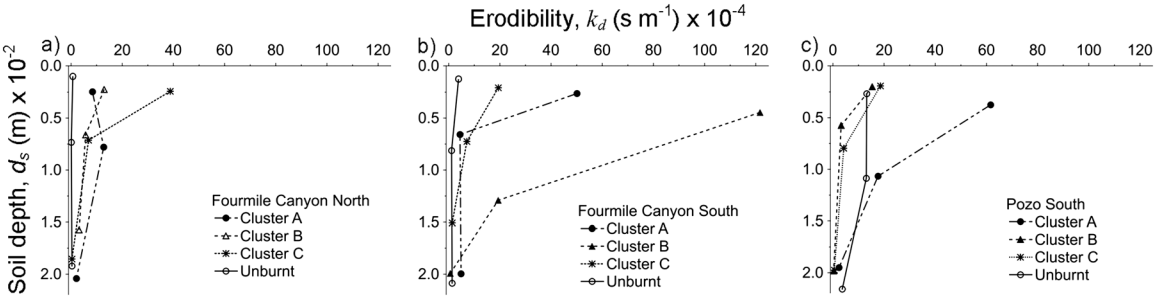

Figure 3. Changes in depth average erodibility, k_d (s m^{-1}), of near-surface soil at (a) Fourmile Canyon North, (b) Fourmile Canyon South, and (c) Pozo South. Three burned samples and one unburned sample are plotted for each site. Each point is the average erodibility obtained from four erosion experiments on four different cores.

[36] Variability in erodibility was analyzed using a general linear model with soil and root variables as predictors. Linear interpolation was used to determine soil and root properties for the exact depth at which erodibility was measured. Soil and root properties at the soil surface were estimated by extrapolating the values measured at 0.01 and 0.02 m. If the extrapolated value was negative, it was given the value of zero. Initially, the linear model included all the measured soil properties (LOI, BD, % silt and clay, RD, and RLD) as part of the analysis. However, the root properties, RD and RLD, were the only variables that emerged as significant predictors. For $d_s < 0.02$ m, the best fit was obtained using RD and d_s as predictors of the log transformed erodibility:

$$\ln(k_d) = \beta_1 + \beta_2 d_s + \beta_3 \mathrm{RD} + \beta_4 d_s \mathrm{RD} + \varepsilon, \quad (5)$$

with $\beta_1 = -5.26$, $\beta_2 = -181$, $\beta_3 = -0.26$, and $\beta_4 = 11.6$. All coefficients were significant ($p < 0.01$) and the overall model explained 62% of the variability in the log transformed k_d ($R^2 = 0.62$, $F_{3,\ 32} = 16.7$, Mean Square Error = 1.89, $p < 0.001$) (Figure 4). A similar but slightly weaker ($R^2 = 0.55$) relation was obtained when RLD was used as predictor instead of RD. In either case, the important result is that the influence of roots on erodibility diminishes with soil depth. For $d_s > 0.02$ m, the best predictor was a constant value of k_d, and the value given by equation (5) for the average value of RD at this depth (6.34 kg m^{-3}) was 1.28×10^{-4} s m^{-1}.

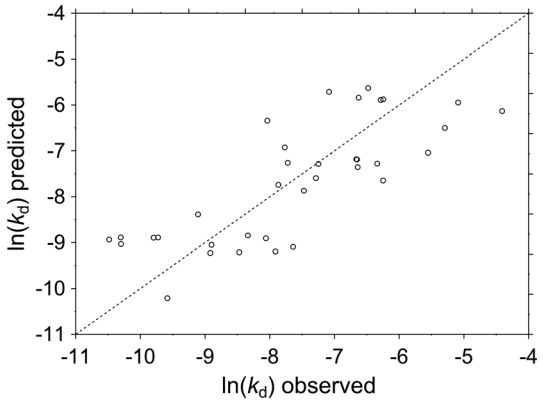

Figure 4. Observed and predicted erodibility, k_d (s m^{-1}), from a general linear model (equation (5)) with depth, d_s (m), and root density, RD (kg m^{-3}), as predictors.

3.2. Temporal Changes in Sediment Availability

[37] Sediment flux measured in the erosion plot experiments at Sunday Creek decreased rapidly with time. For all discharges, the sediment flux per unit width, q_s (kg m^{-1} s^{-1}), decreased by up to two orders of magnitude during the first 20–30 s of erosion (Figure 5). At low unit discharge ($q_w = 1.33$ and 3.33×10^{-3} m^2 s^{-1}), some parts of the surface did not erode during the initial surge of sediment and water, thus creating elevated sections of intact surface material between flow paths. Once established, the flow paths were relatively stable, there was no lateral spread, and q_s appeared to be limited by the detachment rate at the bed of the plot. New material was eroded and flow paths widened once the discharge was increased. This resulted in a return to high q_s, followed by rapid decrease toward a new steady state. Nonsteady flow conditions in the initial stages of erosion for each discharge meant that the flow depth and consequently the total shear stress were changing while the plot was eroding. The calculated shear stress in Table 3 reflects the flow conditions at steady state.

[38] A steady state erodibility value, k_d, of the soil matrix (when $t > 45$ s) was calculated from E to be $1.66 \pm 0.67 \times 10^{-4}$ s m^{-1}(using equation (3) and τ_f instead of τ_{fn}). This value was based on the assumptions that (i) the soil was detachment-limited, and (ii) that deposition was negligible, which were justified because (i) when $t > 45$, the soil was clearly detachment-limited given that sediment flux was low (<0.025 kg m^{-1} s^{-1}) despite the shear stress of the flow (20–50 Pa) being substantially higher than the critical shear stress (~0.5 Pa) for initiation of motion of the majority of particles ($D_{50} = 0.56$ mm), and (ii) the Rouse number ranged from 0.8 to 1.3, so deposition on the plot was likely to be negligible.

[39] During the initial stage of erosion, $q_s(t)$ was found to fit the following exponentially decreasing form (Table 3):

$$q_s(t) = q_{s_{\min}}\left(1 + ae^{-bt}\right) \quad (6a)$$

where a and b are fitted parameters. The asymptote, $q_{s_{\min}}$, is the steady state sediment flux per unit width and is given by

$$q_{s_{\min}} = k_d \tau_f \beta l \quad (6b)$$

where l is the length of the plot and β is the proportion of actively eroding areas which was estimated from the flow width, w, to be 56, 68, and 89% when Q was 2, 5, and 10×10^{-4} m^3 s^{-1}. When $Q = 15 \times 10^{-4}$ m^3 s^{-1}, the full width

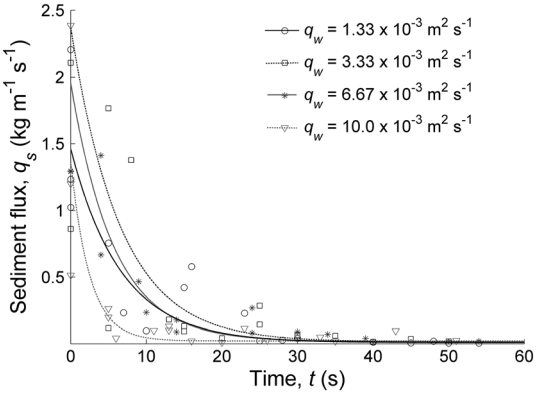

Figure 5. The mean change in sediment flux (q_s) with time (t) with sequentially increasing unit discharge (q_w) in field plots (4 m long and 0.15 m wide) on a burned hillslope at Sunday Creek (southeast Australia). The lines are equation (6a), fit using parameters listed in Table 3.

of the plot was eroding ($w = 0.15$ m) and $\beta = 1$. The exponential term in equation (6a) captures the temporary effects of a finite supply of noncohesive surface soil, which is detached and transported more easily than soil in the underlying matrix where q_s approaches $q_{s_{\min}}$. When fitted to data for each discharge, the function accounted for 63–79% of the variability in q_s for $0 < t < 60$ s.

[40] Equation (6a) represents two stages of the erosion process. Initially, the change in flux with time is proportional to the excess flux, $\frac{\delta q_s}{\delta t} = -b\left(q_s - q_{s_{\min}}\right)$, hence an exponential dependence between q_s and t. However, the available surface material is limited and then exhausted so $\frac{dq_s}{dt} \to 0$ and $q_s \to q_{s_{\min}}$. The magnitude of q_s at $t = 0$ determines the parameter $a = \left[q_{s_{\min}} - q_s(t=0)\right]/q_{s_{\min}}$ and is an estimate of the transport capacity, T_c (kg m^{-1} s^{-1}), which had values ranging from 1.37 to 2.37 kg m^{-1} s^{-1} (Table 3).

[41] Particle-size distribution of eroded material was found to be more dependent on time than on unit discharge. Initially, at $t = 0$ s, the eroded soil contained a large proportion of gravel-sized particles ($9.6 \le D_{50} \le 12$ mm) (Figure 6a). Decrease in particle size with time was more gradual for the intermediate values of q_w than for the lowest and highest q_w. Particle-size distribution averaged for the full experimental period showed an overall coarsening as q_w increased from 1.33 to 6.67×10^{-3} m^2 s^{-1} and a slight fining as q_w increased from 6.67 to 10.0×10^{-3} m^2 s^{-1} (Figure 6b). The relatively small shift in particle-size distribution with increasing unit discharge (Figure 6b) probably reflects preferential depletion of fine material at low discharge rather than increased capacity of the flow to transport the larger particles. This was expected given that the critical shear stress for initiation of motion of the largest particles ($D = 15$ mm, ~11 Pa) is less than 20 Pa which is the minimum steady state τ_f applied in plot experiments [*Wiberg and Smith*, 1987].

[42] The depletion effect on the erosion plots was quantified for each unit discharge by calculating transient yield. The transient yield, Y_t (kg m^{-2}) for each Q was obtained by subtracting $q_{s_{\min}}$ from $q_s(t)$ (using equation (6a)), dividing by the length of the plot, l, and then integrating between 0 and 60 s:

$$Y_t = \frac{\int_0^{60}\left(q_s(t) - q_{s_{\min}}\right)\mathrm{d}t}{l} = k_d \tau_f \beta \int_0^{60} a e^{bt}\mathrm{d}t \tag{7}$$

[43] The sum of transient yield, $\sum Y_t$, for all four levels of Q was 10.8 kg m^{-2}; and the corresponding sum of the steady state yield, $\sum Y_{ss}$, (with constant erodibility $k_d = 1.66 \times 10^{-4}$ s m^{-1}), was 1.0 kg m^{-2}, approximately 10 times less than $\sum Y_t$. Total yield ($\sum Y_t + \sum Y_{ss}$) from the erosion plot (11.8 kg m^{-2}) based on equation (7) corresponds well with the measured total mass of sediment (11.2 kg m^{-2} ± 3.0 SD) measured in 20 L overflow bucket and 0.5 L container bottles. Average depth of erosion measured from erosion pins within the three plots was 0.011 m ± 0.002 SD ($n = 24$). The analysis of sediment yield above indicates that 92% of this material eroded when $q_s > q_{s_{\min}}$. The computed depth of soil contributing to the transient yield is therefore ~0.01 m (i.e., 0.92×0.011 m). This depth is defined as the depth of noncohesive soil, d_{nc} (m).

3.2.1. Linking Sediment Availability to Soil Shear Strength

[44] The depth of noncohesive soil (d_{nc}) was correlated with shear vane measurements in order to determine a shear strength threshold above which the soil is easily eroded by overland flow. Mean values of soil shear strength, τ_v, could be related to the soil depth (Figure 7) by the sigmoid function:

$$\tau_v(d_s) = \frac{\tau_{v_{\max}}}{1.0 + f e^{-p d_s}} \tag{8}$$

[45] The parameter $\tau_{v_{\max}}$ (Pa) is the asymptotic value which τ_v approaches as the depth increases, f is

Table 3. Flow Properties Measured in the Field Plots and the Associated Estimates of Shear Stress and Sediment Flux Parameters

Discharge Q	Unit Discharge q_w	Stream Power[a] Ω	Flow Depth h_w	Flow Velocity u_{dye}	Flow Width[b] w	Shear Stress[c] τ_f	Steady Flux $q_{s_{\min}}$	Fitted Parameters[d] a	b	R^2	Transport Capacity[e] T_c
($m^3 s^{-1} \times 10^{-4}$)	($m^2 s^{-1} \times 10^{-3}$)	(Pa s^{-1})	(m × 10^{-2})	(m s^{-1})	(m × 10^{-1})	(Pa)	(kg m^{-1} s^{-1})	-	(s^{-1})		(kg m^{-1} s^{-1})
2	1.33	0.75	0.6	0.62	0.8	22	0.010	145	0.150	0.78	1.46
5	3.33	1.88	1.0	0.80	1.0	35	0.015	157	0.152	0.61	2.37
10	6.67	3.76	1.2	1.03	1.3	40	0.017	114	0.172	0.70	1.96
15	10.0	5.65	1.4	1.14	1.5	50	0.022	61.1	0.400	0.67	1.37

[a]Stream power, $\Omega = \rho g Q S$.
[b]Mean flow width $w = Q/(h_w \overline{u})$, where $\overline{u}$ is the mean cross-sectional velocities of the flow, $\overline{u} = 0.63\, u_{dye}$.
[c]Shear stress calculated based on the flow conditions once q_s had reached steady state.
[d]Parameter values from equation (6a) and fitted functions in Figure 5.
[e]Transport capacity calculated using $T_c = q_{s_{\min}}(1 + a)$ from equation (6a). Note that these values were obtained in a succession of increasing discharge, and therefore incorporate the effects of depletion by the previous lower levels of discharge on the plot.

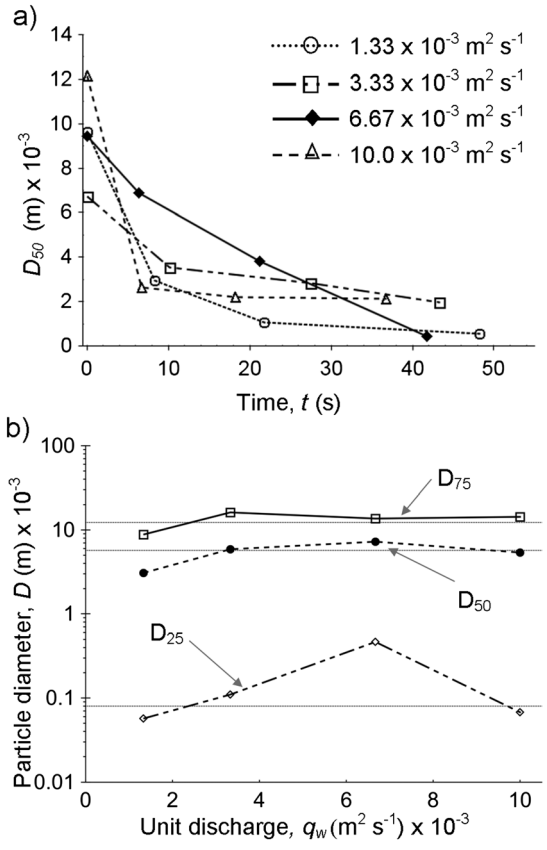

Figure 6. (a) Median particle diameter (D_{50}) of eroded sediment for different levels of discharge applied sequentially to a confined test area on steep slopes (36–38%) burned at high severity. The particle-size distribution was averaged in temporal bins corresponding to four time intervals. (b) The particle-size distribution as a function of sequentially increasing unit discharge (q_w) shown using the median (D_{50}), upper (D_{75}), and lower (D_{25}) quartiles of the distribution. The overall particle-size distribution for all sediment produced during the 60 s experimental period is shown as solid lines.

essentially the dimensionless ratio of $\tau_{v_{max}}$ to τ_v when $d_s = 0$, $\left(1 + f = \frac{\tau_{v_{max}}}{\tau_v(d_s=0)}\right)$, and p (m^{-1}) determines the rate of change of τ_v with change in d_s. This function accounted for 99% of variability in mean value of τ_v with d_s ($\tau_{v_{max}} = 35.7$ kPa, $f = 21.6$; $p = 1.25\ m^{-1}$). The strong gradient in τ_v between d_s equal to 0.01 and 0.03 m shows that surface and subsurface soil display very different properties: an easily eroded and noncohesive surface layer with low shear strength overlying a resistant and cohesive subsurface layer.

[46] The threshold value of τ_v at the transition from noncohesive to cohesive soil was obtained by using equation (8) to calculate $\tau_v(d_s)$ for $d_s = d_{nc} = 0.01$ m (i.e., the depth of the noncohesive soil layer in the adjacent erosion plot). The τ_v threshold was 5 kPa (Figure 7). This soil shear strength value corresponds to a critical flow shear stress of ~1.3 Pa [*Léonard and Richard*, 2004, equation (7)], which is in the upper range of critical shear stress values reported for soils that were affected by temperatures >250°C [*Moody et al.*, 2005], and it is higher than the noncohesive threshold for agricultural soils (1 kPa) [*Morgan et al.*, 1998; *Rauws and Covers*, 1988] having fine sediment ($D_{50} = 0.25$–0.60 mm) and comparatively low slopes (0.035–0.16).

3.3. Availability of Noncohesive Soils in Burned Headwaters

[47] The soil shear strength threshold for noncohesive soil was used to quantify the depth of noncohesive soil in the headwaters at Ella Creek, Sunday Creek, and Stony Creek during recovery from wildfire. The dependence of the soil shear strength on depth for different stages of recovery was well represented by equation (8) ($R^2 = 0.94$–0.99) (Figure 8 Table 4). Variability at each depth was often high as shown by the large standard deviation (Figure 8). At the two most recently burned sites (Sunday Creek and Stony Creek), the soil shear strength at the soil surface ($d_s = 0$) in September (0.5 years after fire) was low ($\tau_v = 1.2$–1.7 kPa, Table 4), homogenous (SD ranging from 0.8 to 0.9 kPa), and similar (Figures 8a and 8b, Table 4). It increased to 3–4 kPa at $d_s = 0.01$ m and became more variable (SD ranging from 2.9 to 3.2 kPa). Soil shear strength of surface soils increased markedly in the 0.5 year period between September 2009 and March 2010. At Stony Creek in March 2010 (1 year after the wildfire), there was no discrete surface layer of noncohesive erodible soil, such that the shear strength on the soil surface was higher (12.2 ± 5.6 kPa), and there was a linear (as opposed to sigmoid) increase in τ_v with d_s between the soil surface and $d_s = 0.03$ m. Sunday Creek displayed a more modest increase in surface τ_v from September 2009 ($\tau_v = 2.4$ kPa) to March 2010 ($\tau_v = 7.1 \pm 6.5$ kPa). At Ella Creek (burned 2007), the soil remained more or less unchanged between September 2009 (2.5 years since the wildfire) and March 2010 (3 years since the wildfire) so that a single function was used to represent both sets of measurements (Figure 8c). Average τ_v at the soil surface for both measurement campaigns at Ella Creek was 11.4 ± 9.1 kPa, and there was a linear increase in τ_v for d_s between 0 and 0.03 m.

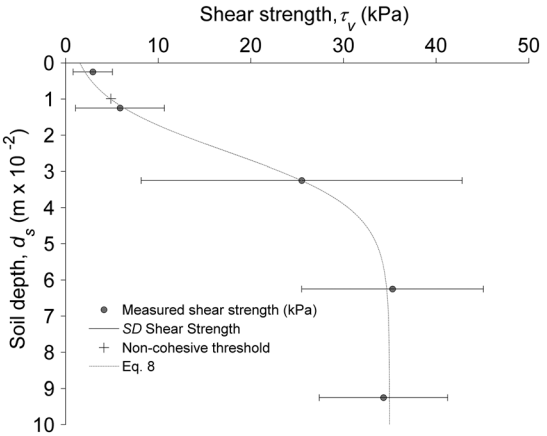

Figure 7. Mean soil shear strength (τ_v) and standard deviation (*SD*) as a function of soil depth (d_s) for 15 sample points along the outside edge of the erosion plots at Sunday Creek. The depth of noncohesive soil, d_{nc}, was used to define the point (+) along the fitted equation (8) where the soil shear strength marks a transition from noncohesive to cohesive material.

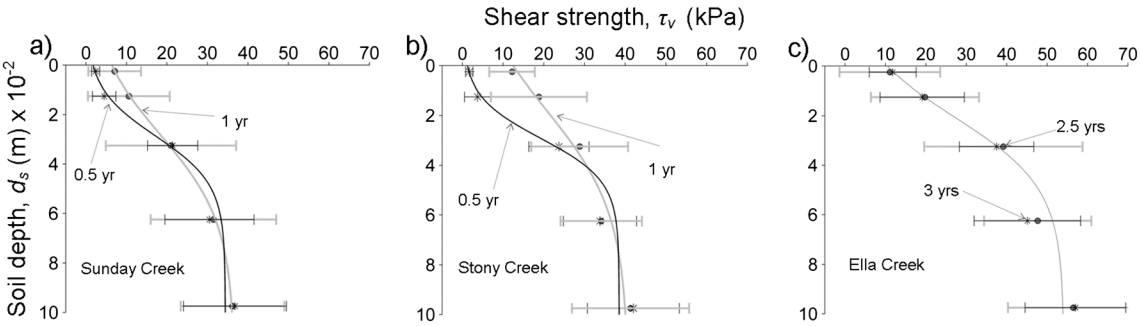

Figure 8. Changes in soil shear strength (τ_v) with soil depth (d_s) at different stages of recovery after wildfire (September 2009 and March 2009) at (a) Sunday Creek ($n = 50$) (b) Stony Creek ($n = 27$), and (c) Ella Creek ($n = 27$). The soil shear strength at 0.5 years since wildfire was measured on noneroded sections of the hillslope and therefore represents the surface properties without depletion effects that may have taken place between the initial wildfire impact and the sampling campaign (i.e., taken to represent conditions immediately following the burn). At Sunday Creek and Stony Creek, the number of sampling points was about 10% lower for d_s at 6.5 and 10 cm, due to the rock and gravel encountered during sampling. Bars represent one standard deviation.

[48] The depth of the noncohesive layer (d_{nc}) in the sampled headwaters was obtained from the shear vane measurements by calculating the proportion of noncohesive soil as a function of depth. Assuming a noncohesive threshold of 5 kPa (see section 3.2), the proportion of noncohesive soil ($\tau_v < 5$ kPa) was calculated at each sampling depth (Figure 9a). At Sunday Creek and Stony Creek, all the sampled points were noncohesive on noneroded surfaces 6 months after the wildfire. One year after the wildfire, this had decreased to 54 and 17% for Sunday Creek and Stony Creek, respectively. Less than 20% of surface soil was noncohesive at Ella, 2.5 to 3 years after the wildfire. An exponential cumulative distribution function $\left(\text{CDF} = 1 - e^{\lambda d_s}\right)$ was fit to the cumulative proportion of noncohesive soil with increasing d_s ($R^2 = 0.84$–0.98) and plotted as a probability density function (PDF) in Figure 9b. All soil particles at $d_s = 0$ were assumed to be noncohesive in the fitting procedure. The expected value of the PDF, $E[d_s] = 1/\lambda$, is the average depth of noncohesive soil (d_{nc}), which can be represented by a two-parameter exponential decay function ($R^2 = 0.96$) of time since fire, t_{sf} (years), (Figure 9c)

$$d_{nc} = d_{nc(t=0)} e^{-rt_{sf}} \tag{9}$$

[49] These parameters are the initial estimates of the production (by wildfire) of noncohesive soil, ($d_{nc(t=0)} = 0.89$ m) and the rate of decline in availability ($r = 1.59$ y^{-1}). The particle size, loss on ignition, and solubility of the noncohesive material at Sunday Creek and Stony Creek are given in Table 5.

Table 4. Shear Strength Parameters in Equation (8) Based on Data From Surveys in Small Headwaters of Sunday Creek, Stony Creek, and Ella Creek in Southeast Australia

Site	Time Since Fire t_{sf} (years)	Parameters $\tau_{v_{max}}$ (kPa)	f	p (m^{-1})	Adjusted R^2	Shear Strength ($d_s = 0$) τ_v (d_s) (kPa)
Sunday Creek	0.5	34.4	18.8	1.02	0.96	1.7
	1.0	36.7	4.76	0.56	0.99	6.4
Stony Creek	0.5	38.5	30.6	1.17	0.95	1.2
	1.0	40.8	2.28	0.47	0.96	12.4
Ella	2.5	55.3	3.65	0.55	0.94	11.9
	3.0	54.1	4.16	0.70	0.97	10.5

4. Discussion

4.1. Effect of Roots on Erodibility

[50] Burn impacts on soil physical and hydraulic properties have been linked to fire severity [*DeBano et al.*, 2005; *Hungerford et al.*, 1991; *Parsons et al.*, 2010]. However, no explicit link has been drawn between burn impacts and the erodibility of the soil. This study showed that the average surface erodibility of a noncohesive layer on burned hillslopes ranged from 20.0×10^{-4} to 63.7×10^{-4} s m^{-1} and depended on the density of fine roots (<2 mm diameter). These values are high, and result in high detachment rates that can provide material for the progressive bulking of debris flows [e.g., *Cannon et al.*, 2001; *Gabet and Bookter*, 2008; *Nyman et al.*, 2011]. Below the highly erodible noncohesive layer, the erodibility of the cohesive layer appears to be similar for a variety of locations throughout the world. For example, the erodibility (measured in the flume experiments) for fire-affected soils from three sites in the western United States ranged from 1.48 to 2.03×10^{-4} s m^{-1} and was similar in magnitude to the steady state erodibility measured in the erosion plots at Sunday Creek in southeastern Australia (1.66×10^{-4} s m^{-1}) and similar to steady state erodibility reported for high-severity wildfires in the northwestern United States (e.g., 2.0×10^{-4} s m^{-1} [*Wagenbrenner et al.*, 2010]). These values of erodibility for the two layers provide critical parameters for developing a two-layer model of postwildfire erosion.

[51] Roots reinforce the soil matrix by providing extra cohesion in addition to the intrinsic cohesion of soil aggregates [*De Baets and Poesen*, 2010; *Fattet et al.*, 2011; *Gyssels et al.*, 2005]. The statistical model in equation (5) indicates that fire-induced changes to erodibility can be predicted using root density, which may be

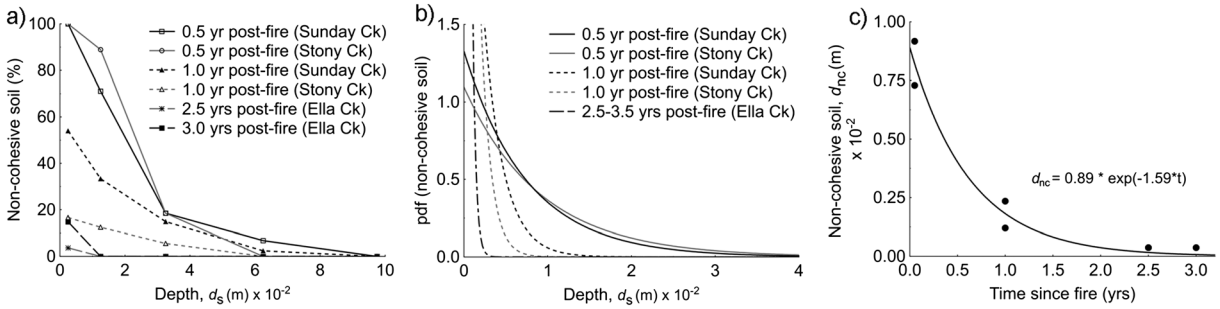

Figure 9. (a) The percentage noncohesive soil plotted as function of depth (d_s) by applying a soil shear strength (τ_v) threshold of 5 kPa. The threshold was defined based on the average depth of soil removed from the erosion plot experiments at Sunday Creek. (b) A cumulative density function was fit to the data in Figure 9a and is presented as a probability density function (PDF). (c) The expected depth $E[d_s]$ of the PDF in Figure 9b as a measure of the average depth of noncohesive soil, d_{nc}, (m) as a function time (years) since fire (t_{sf}).

directly related to heat impacts on the soil [*Parsons et al.*, 2010]. The exponential decrease in the influence of roots with depth is probably due to (i) a natural decrease in fibrous root density, (ii) a decrease caused by the necrosis of roots [*Michaletz and Johnson*, 2007; *Smirnova et al.*, 2008], and (iii) the increase in the influence of other soil properties such as percentage silt and clay or bulk density, which correlated with erodibility at $d_s > 0.03$ m. This pattern is consistent with observations by *DeBano et al*, [2005] that at greater soil depths the amount of organic matter decreases and interparticle bonds become increasingly important as sources of soil structure and cohesion.

[52] At the soil surface, the variability in erodibility of the burned soils from three sites in the western United States was almost identical with coefficient of variation (CV) ranging from 0.81 to 0.82. This variability at scales $<1\,m^2$ is greater than the variability between the three sites (CV = 0.59). Further analysis of variability shows that the ratio of CV between samples to CV between sites decreases with soil depth, which means that the influence of site factors on erodibility increase with depth. This supports the notion that wildfire can "homogenize" the landscape [e.g., *Ebel*, 2012] and that surface properties become independent of some of the specific geological and pedological factors which contribute to variability between sites [*Sheridan et al.*, 2000; *Tisdall and Oades*, 1982; *Wischmeier and Mannering*, 1968].

Table 5. Properties of Noncohesive Material d_{nc} at Sunday Creek and Stony Creek

		Sunday Creek	Stony Creek
Loss on Ignition[a] (%)		23.6	7.3
Solubility[b] (%)		2.3	1.9
Particle Size[c] (mm)			
Gravel (%)	>2	54	31
Coarse & Medium Sand (%)	0.250-2	7.5	2.5
Fine Sand (%)	0.063-0.250	14.1	15.2
Silt (%)	0.002-0.063	22.5	47.5
Clay (%)	<0.002	1.9	3.7

[a]Percent mass loss after heating at 500°C for 2 h.
[b]Solubility measured as the percentage mass loss after submerging 5 g of material (<2 mm) in 2 L of distilled water at 20°C for 48 h.
[c]Particle-size distribution determined using laser diffraction particle-size analyzer with a sonicator but no dispersing agent.

4.2. Sediment Depletion and Transient Conditions on Burned Hillslopes

[53] Postwildfire erodibility can be simplified into a two-layer model with a noncohesive layer overlying a cohesive substrate. The noncohesive layer lacks structure and has been shown to consist of ash, partially combusted organics, gravel, and mineral soil [*Badia and Marti*, 2003; *Moody and Ebel*, 2012; *Woods and Balfour*, 2010], and the depth of this noncohesive layer, d_{nc}, can be determined by measuring the soil shear strength. Essentially, no detachment is required to initiate erosion within the noncohesive layer because typical shear stresses on steep hillslopes exceed the critical shear stress necessary to initiate motion and resuspension, therefore resulting in transient and potentially transport-limited conditions [*Hairsine and Rose*, 1992; *Rauws and Covers*, 1988; *Zhang et al.*, 2009]. However, this noncohesive layer can be depleted [*Ziegler et al.*, 2000]. Depletion results in a strong temporal shift in the composition of the eroded soil (Figure 6a) and is associated with a strong reduction in the sediment flux (Figure 5).

[54] The exponential decline of noncohesive depth, d_{nc}, during recovery (Figure 9c), indicates that the d_{nc} parameter was responsive to fire-related impacts on sediment availability and recovery of the soil. Initially, after the wildfire, the entire surface in the sampled headwaters at Sunday Creek and Stony Creek consisted of noncohesive layer. The average depth of this layer was estimated to be between 0.007 and 0.009 m (7–9 mm). With an average bulk density of 1300 kg m^{-3} (measured for soil depths between 0 and 0.02 m), this depth equates to 97–117 Mg ha^{-1} of noncohesive material, which is readily available for transport on recently burned hillslopes. Failing to incorporate this source of material as a part of the overall sediment availability could be an important source of error in existing models that are used to predict postwildfire erosion. After 2.5–3 years since fire (in the Ella Creek catchment), the d_{nc} was reduced to a thin layer of noncohesive soil (<5 Mg ha^{-1}), essentially corresponding to a single-particle layer. Once the noncohesive layer was depleted, the erosion process shifted toward detachment-limited conditions where the sediment flux was steady and determined by flow properties and a constant erodibility of the cohesive layer. The shift from transient to steady state conditions corresponded to a threefold shift in soil shear strength between soil depths of 0.01 and 0.03 m.

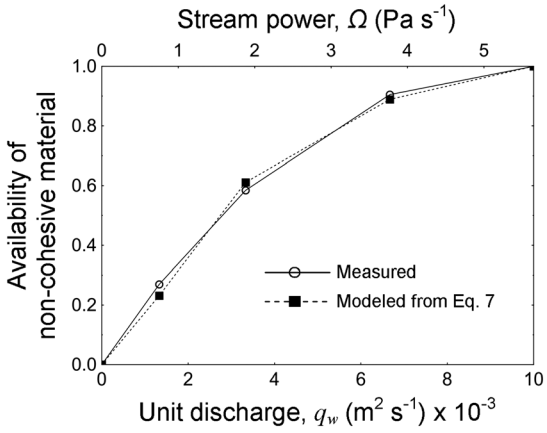

Figure 10. The cumulative availability of sediment as a function of unit discharge (q_w) and the stream power (Ω). The plots are generated from (i) measurements of sediment yield ($kg\,m^{-2}$) and (ii) modeled sediment yield (equation (7)) from the fitted sediment flux functions in Figure 5.

[55] Sediment yield produced during transient conditions was a function of discharge. Transient sediment yield, Y_t, during the initial flux was 2.5, 4.1, 3.0, and 1.2 $kg\,m^{-2}$ when the unit discharge was increased sequentially from 1.33 to $10.0 \times 10^{-3}\,m^2\,s^{-1}$. Increased cumulative yield with increasing discharge on the erosion plot can be interpreted as an increased potential to erode a finite pool of material in the noncohesive layer. At each new discharge, an increasing proportion of the noncohesive material was entrained and transported off the plot (Figure 10). The dominance of large particles in the initial flux of water and sediment from the field erosion plots (Figure 6a) indicates that the steep flow front may result in an increased flow competence, an effect which may have been amplified by potential increase in viscosity due to the high concentration of fine sediment in the flow [*Gabet and Sternberg*, 2008; *Rickenmann*, 1991], or perhaps by the fact that the critical shear stress is less for particle diameters that are greater than the typical height of the bed roughness on which they are moving (i.e., the relative roughness is small) [*Wiberg and Smith*, 1987].

[56] While the effect of steep flow fronts is an artifact of the experimental design (i.e., step-wise increase in flow), it is a realistic representation of the dominant erosion processes operating on steep hillslopes exposed to short duration and high intensity rainfall [*Horton*, 1945; *Schumm*, 1956; *Wondzell and King*, 2003]. Pulses of flow, appropriately described by *Horton* [1945] as "rain wave trains", are a form of nonuniform flow caused by accelerating flow and by the build up and bursting of small sediment or debris dams. Steep flow fronts, the potentially high sediment concentration in flow pulses, and the relative roughness of the bed can lead to flow competence and transport capacity in excess of what is captured during steady state erosion experiments in flumes [*Gabet and Sternberg*, 2008]. Using traditional measures of transport capacity [e.g., *Foster and Meyer*, 1972; *Govers*, 1990; *Zhang et al.*, 2005] may therefore be misleading when modeling hillslope erosion during high intensity rainfall in burned systems.

4.3. Large-Scale Implication: A Conceptual Model

[57] The interplay between background erodibility and the influence of wildfire on sediment availability can have important implication for the type and magnitude of postwildfire erosion responses. For instance, *Larsen et al.* [2006] showed that the frequency of debris flows was insensitive to fire effects on weathering-limited systems with low sediment availability on hillslopes. Similarly, *Nyman et al.* [2011] found that weathering-limited catchments in plutonic granite terrain in northeast Victoria (southeast Australia) were less susceptible to runoff generated debris flows after wildfire than the adjacent sedimentary catchments. Sedimentary catchments were not weathering-limited, and the soil mantled hillslopes in these systems provided a major source of fine sediment for postwildfire debris flows [*Smith et al.*, 2012]. *Cannon et al.* [2003] observed a similar pattern where the presence of noncohesive soil on hillslopes resulted in earlier initiation of debris flows than on hillslopes with less available sediment. These studies indicate that explicit representation of wildfire effects on sediment availability is important for predicting both type and magnitude of erosion responses on burned hillslopes.

[58] Results from this study can be used to develop a conceptual framework for quantifying wildfire effects more broadly across systems with different soils and vegetation (Figure 11). The most fundamental relation is the dependency between erodibility and the availability of noncohesive material on the surface (Figure 11a), a dependency which will appear stronger for soils with low background erodibility. The magnitude of the changes in erodibility caused by fire effects in relation to background erodibility ultimately determines the sensitivity of geomorphic systems to wildfire in terms of sediment availability. The role of wildfire in driving the dependency between erodibility and availability of noncohesive material can be captured by modeling the production and depletion of noncohesive soil. Initial production is a function of fire severity, while the return to prefire conditions can take different trajectories depending on the local factors that affect depletion through erosion and soil recovery (Figure 11b). Representing fire effects as perturbations above the background conditions provides a basis for understanding the role of sediment availability in modulating postwildfire erosion responses across variable landscapes [*Prosser and Williams*, 1998].

5. Conclusions

[59] Sediment availability was investigated at the point scale in the laboratory and at the hillslope and catchment scale in the field. At the point scale, root properties were found to be an important variable that can be used to predict the erodibility of fire-affected soil. Specifically, root density and soil depth accounting for 62% of the variation in erodibility. This provides an explicit link between sediment availability and a root property that is directly impacted by burning. Postwildfire sediment availability and erodibility vary spatially and temporally. In fire-affected soils, erodibility at the point scale decreased exponentially with depth through a layer of noncohesive soil and ash. This layer potentially provides an important source of material during the postwildfire period, particularly immediately after the initial burn impact.

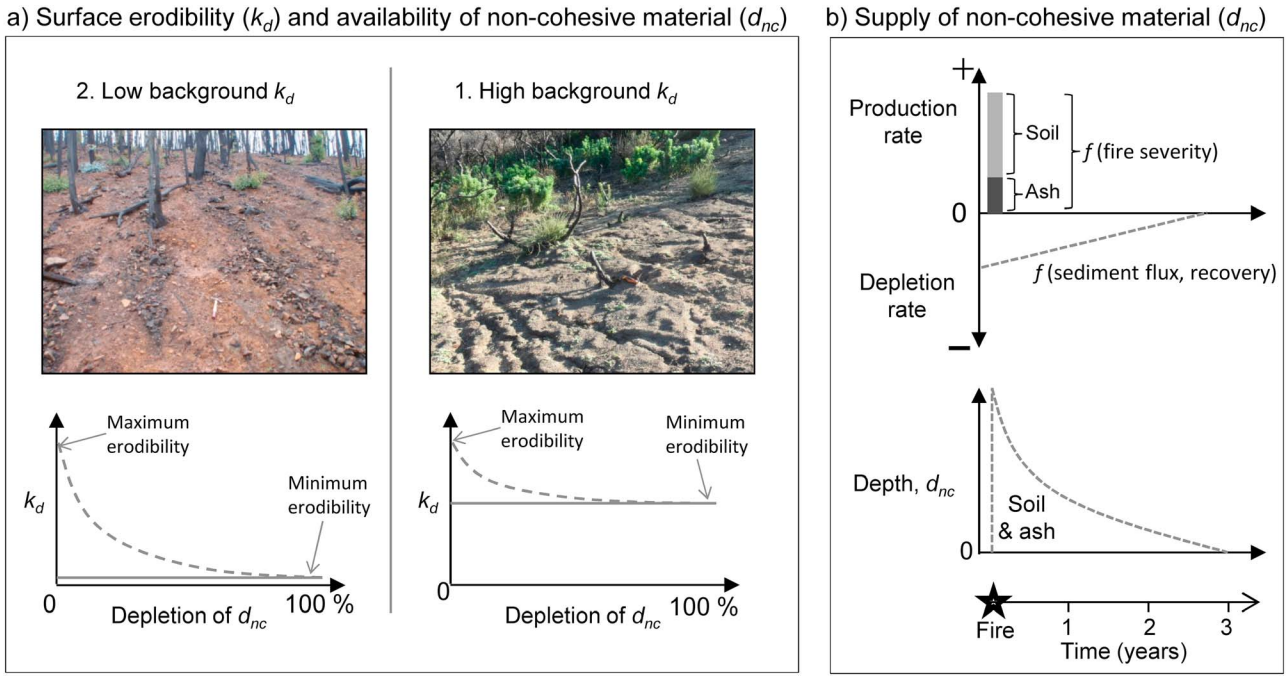

Figure 11. Conceptual model of sediment availability on burned hillslopes. (a) The surface erodibility is a function of background erodibility and the availability of noncohesive soil. With a complete cover of noncohesive soil, the erodibility is at a maximum. When noncohesive material is depleted, the erodibility decreases to background levels. (b) The initial fire effect and the subsequent recovery are represented through the production and depletion of noncohesive soil. These processes determine the depth of noncohesive material at any point in time. For a low-severity fire, the production of noncohesive soil is minimal, it is rapidly depleted, and the perturbation to k_d is therefore small. The low and high background erodibility scenarios in Figure 11a represent hillslopes from Sunday Creek, southeast Australia (clay loam soil) and Arroyo Seco, California (sandy soil) [see *Kean et al.*, 2011].

[60] Instead of measuring steady state erodibility of burned hillslopes, this paper focused on the transient erodibility of the noncohesive layer. Initially, erodibility and sediment flux from the noncohesive layer were high and independent of the background erodibility. With time, the availability of noncohesive soil was depleted and sediment flux trended back toward a steady state with a constant erodibility between 1.0 and $2.0 \times 10^{-4}\,\mathrm{s\,m^{-1}}$ as erosion reached the cohesive layer. Measurements of soil shear strength was correlated with the shift from noncohesive to noncohesive soils and provided a practical method to estimate the thickness of the noncohesive layer at the field scale. Changes in sediment availability during recovery could be represented spatially as a probability distribution of noncohesive soil depth with a mean that decreases exponentially with time since wildfire.

[61] This paper presents a conceptual model of sediment availability with explicit representation of the noncohesive surface layer that is produced by wildfire. The conceptual model provides an opportunity to explore changes in sediment availability in context of fire severity, soil heating, and the interaction with intrinsic catchment properties such as soil, geology, and vegetation. The model can also be coupled with information on fire effects on runoff to evaluate the relative importance of sediment availability versus runoff generation mechanisms to determine how different geomorphic systems respond to wildfire.

[62] Linking the roots properties in near-surface soils with burn severity and the depth distribution of noncohesive material is a particularly interesting avenue for future research, which may provide useful insight into the quantitative link between fire behavior, soil heating, and sediment availability on hillslopes. Another research avenue is to develop a quantitative basis for representing ash as an input to sediment availability, so that erosion rates from burned catchments can be evaluated in context of this additional source of sediment, which is unrelated to weathering.

Notation

LOI	loss on ignition	nondimensional
BD	bulk density	$\mathrm{kg\,m^{-3}}$
RD	root density	$\mathrm{kg\,m^{-3}}$
RLD	root-length density	$\mathrm{m\,m^{-3}}$
Q	discharge	$\mathrm{m^3\,s^{-1}}$
S	friction slope	nondimensional
ρ	density of water	$\mathrm{kg\,m^{-3}}$
g	acceleration due to gravity	$\mathrm{m\,s^{-2}}$
h_w	water depth	m
τ_f	uniform flow shear stress	Pa
h_{w1}	water depth (first point gauge)	m
h_{w2}	water depth (second point gauge)	m
$\overline{u}_1$	average flow velocity(first point gauge)	$\mathrm{m\,s^{-1}}$
$\overline{u}_2$	average flow velocity(second point gauge)	$\mathrm{m\,s^{-1}}$
d	distance between point gauges	m
τ_{fn}	nonuniform flow shear stress	Pa

E	detachment rate	$kg\,m^{-2}\,s^{-1}$
d_s	depth below the soil surface	m
k_d	erodibility	$s\,m^{-1}$
q_s	sediment flux per unit width	$kg\,m^{-1}\,s^{-1}$
t	time	seconds
u_{dye}	flow velocity from dye	$m\,s^{-1}$
w	flow width	m
$\overline{u}$	average flow velocity on bounded field plots	$m\,s^{-1}$
α	coefficient for calculating average flow velocity	nondimensional
q_w	unit discharge	$m^2\,s^{-1}$
Ω	stream power	$Pa\,s^{-1}$
D	particle diameter	m
τ_v	vane shear strength	Pa
$q_{s_{min}}$	q_s at steady state	$kg\,m^{-1}\,s^{-1}$
l	length of erosion plot	m
β	proportion of area actively eroding	nondimensional
a	sediment flux parameter	nondimensional
b	sediment flux parameter	s^{-1}
Y_t	transient yield	$kg\,m^{-2}$
Y_{ss}	steady state yield	$kg\,m^{-2}$
d_{nc}	depth of noncohesive soil	m
$\tau_{v_{max}}$	maximum vane shear strength	Pa
f	shear strength parameter	nondimensional
p	shear strength parameter	m^{-1}
λ	distribution parameter for noncohesive soil	m^{-1}
t_{sf}	time since fire	years
$d_{nc(t=0)}$	production of noncohesive soil by fire	m
r	depletion rate of noncohesive material	$years^{-1}$

[63] **Acknowledgments.** The study was conducted as part of a postgraduate scholarship from Melbourne Water and the eWater CRC. Travel and research expenses in the U.S. were funded by the USGS and the University of Melbourne overseas research experience scholarship. Many thanks to Deborah Martin for sourcing literature and to Pierce Martin for his laboratory assistance. Fieldwork in SE Australia was conducted with support from Wim Bovill and Paul McCann. Field work in Colorado was expedited by John Smeins (BLM), Erin Watkins (BLM), and Eric Schroeder (USFS), and fieldwork in California was facilitated by Melody Fountain (USFS). Dick Martin (Martin Entreprise) was instrumental in designing and fabricating parts for the tilting flume while Graeme Scheuber (RMIT) assisted with flume illustrations. The manuscript has benefited from comments and suggestions from anonymous reviewers and the Editor.

References

Al-Hamdan, O. Z., F. B. Pierson, M. A. Nearing, C. J. Williams, J. J. Stone, P. R. Kormos, J. Boll, and M. A. Weltz (2012), Concentrated flow erodibility for physically based erosion models: Temporal variability in disturbed and undisturbed rangelands, *Water Resour. Res.*, *48*, W07504, doi:10.1029/2011WR011464.

Badia, D., and C. Marti (2003), Plant ash and heat intensity effects on chemical and physical properties of two contrasting soils, *Arid Land Res. Manage.*, *17*(1), 23–41.

Blake, W. H., I. G. Droppo, G. S. Humphreys, S. H. Doerr, R. A. Shakesby, and P. J. Wallbrink (2007), Structural characteristics and behavior of fire-modified soil aggregates, *J. Geophys. Res.*, *112*, F02020, doi:10.1029/2006JF000660.

Bryan, R. B. (2000), Soil erodibility and processes of water erosion on hillslope, *Geomorphology*, *32*(3–4), 385–415, doi:10.1016/s0169-555x(99)00105-1.

Cannon, S. H., E. R. Bigio, and E. Mine (2001), A process for fire-related debris flow initiation, Cerro Grande fire, New Mexico, *Hydrol. Processes*, *15*(15), 3011–3023, doi:10.1002/hyp.388.

Cannon, S., J. E. Gartner, C. Parrett, and M. Parise (2003), Wildfire-related debris-flow generation through episodic progressive sediment-bulking processes, western USA, paper presented at Debris-Flow Hazards Mitigation - Mechanics, Prediction, and Assessment, in *Proceedings of the Third International Conference on Debris-Flow Hazards Mitigation*, edited by D. Rickenmann and C. L. Chen, pp. 71–82, Millpress, Davos, Switzerland.

Cerdà, A., and S. H. Doerr (2008), The effect of ash and needle cover on surface runoff and erosion in the immediate post-fire period, *Catena*, *74*(3), 256–263, doi:10.1016/j.catena.2008.03.010.

Cerda, A., and T. Lasanta (2005), Long-term erosional responses after fire in the Central Spanish Pyrenees - 1 Water and sediment yield, *Catena*, *60*(1), 59–80, doi:10.1016/j.catena.2004.09.006.

Chorley, R. J. (1959), The geomorphic significance of some Oxford soils, *Am. J. Sci.*, *257*(7), 503–515, doi:10.2475/ajs.257.7.503.

Cruz, M. G., A. L. Sullivan, J. S. Gould, N. C. Sims, A. J. Bannister, J. J. Hollis, and R. J. Hurley (2012), Anatomy of a catastrophic wildfire: The Black Saturday Kilmore East fire in Victoria, Australia, *For. Ecol. Manage.*, *284*, 269–285, doi:10.1016/j.foreco.2012.02.035.

De Baets, S., and J. Poesen (2010), Empirical models for predicting the erosion-reducing effects of plant roots during concentrated flow erosion, *Geomorphology*, *118*(3-4), 425–432, doi:10.1016/j.geomorph.2010.02.011.

De Baets, S., J. Poesen, G. Gyssels, and A. Knapen (2006), Effects of grass roots on the erodibility of topsoils during concentrated flow, *Geomorphology*, *76*(1-2), 54–67, doi:10.1016/j.geomorph.2005.10.002.

DeBano, L. F., D. G. Neary, and P. F. Ffolliott (2005), Chapter 2: Soil physical properties, in *Wildland Fire in Ecosystems: Effects of Fire on Soils and Water*, edited by D. G. Neary, K. C. Ryan, and L. F. DeBano, pp. 29–52, U.S. Department of Agriculture Forest Service, Rocky Mountain Research Station, Ogden, Utah.

Doerr, S. H., R. A. Shakesby, W. H. Blake, C. J. Chafer, G. S. Humphreys, and P. J. Wallbrink (2006), Effects of differing wildfire severities on soil wettability and implications for hydrological response, *J. Hydrol.*, *319*(1-4), 295–311.

Ebel, B.(2012), Wildfire impacts on soil-water retention in the Colorado Front Range, United States, *Water Resour. Res.*, *48*, W12515, doi:10.1029/2012WR012362.

Ebel, B. A., J. A. Moody, and D. A. Martin (2012), Hydrologic conditions controlling runoff generation immediately after wildfire, *Water Resour. Res.*, *48*, W03529, doi:10.1029/2011WR011470.

Elliot, W. J., A. M. Liebenow, J. M. Laflen, and K. D. Kohl (1989), A compendium of soil erodibility data from WEPP cropland soil field erodibility experiments 1987 & 1988, *Rep.3*, Natl. Soil Erosion Res. Lab., West Lafayette, Indiana.

Fattet, M., Y. Fu, M. Ghestem, W. Ma, M. Foulonneau, J. Nespoulous, Y. Le Bissonnais, and A. Stokes (2011), Effects of vegetation type on soil resistance to erosion: Relationship between aggregate stability and shear strength, *Catena*, *87*(1), 60–69, doi:10.1016/j.catena.2011.05.006.

Foltz, R. B., H. Rhee, and W. J. Elliot (2008), Modeling changes in rill erodibility and critical shear stress on native surface roads, *Hydrol. Processes*, *22*(24), 4783–4788, doi:10.1002/hyp.7092.

Foster, G. R. (1995), Hillslope erosion component, *Rep.10*, 11.11–11.12 pp, Natl. Soil Erosion Res. Lab, West Lafayette, Indiana.

Foster, G. R., and L. D. Meyer (1972), A closed-form soil erosion equation for upland areas, in *Sedimentation: Symp. to Honor Prof. H.A. Einstein*, edited by H. Shen, pp. 2.1–12.17, Colorado State University, Fort Collins, CO.

Gabet, E. J. (2003), Post-fire thin debris flows: Sediment transport and numerical modelling, *Earth Surf. Processes Landforms*, *28*(12), 1341–1348, doi:10.1002/esp.590.

Gabet, E. J., and A. Bookter (2008), A morphometric analysis of gullies scoured by post-fire progressively bulked debris flows in southwest Montana, USA, *Geomorphology*, *96*(3-4), 298–309, doi:10.1016/j.geomorph.2007.03.016.

Gabet, E. J., and A. Bookter (2011), Physical, chemical and hydrological properties of Ponderosa pine ash, *Int. J. Wildland Fire*, *20*(3), 443–452, doi:10.1071/WF09105.

Gabet, E. J., and P. Sternberg (2008), The effects of vegetative ash on infiltration capacity, sediment transport, and the generation of progressively bulked debris flows, *Geomorphology*, *101*(4), 666–673, doi:10.1016/j.geomorph.2008.03.005.

Giovannini, G., and S. Lucchesi (1983), Effect of fire on hydrophobic and cementing substances of soil aggregates, *Soil Sci.*, *136*(4), 231–236.

Gould, S. F. (1998), Proteoid root mats bind surface materials in Hawkesbury Sandstone biomantles, *Soil Res.*, *36*(6), 1019–1032, doi:10.1071/S98004.

Govers, G. (1990), Empirical relationships on the transporting capacity of overland flow, *Int. Assoc. Hydrol. Sci.*, *189*, 45–63.

Govers, G., W. Everaert, J. Poesen, G. Rauws, J. De Ploey, and J. P. Lautridou (1990), A long flume study of the dynamic factors affecting the resistance of a loamy soil to concentrated flow erosion, *Earth Surf. Processes Landforms*, *15*(4), 313–328, doi:10.1002/esp.3290150403.

Grabowski, R. C., I. G. Droppo, and G. Wharton (2011), Erodibility of cohesive sediment: The importance of sediment properties, *Earth Sci. Rev.*, *105*(3-4), 101–120, doi:10.1016/j.earscirev.2011.01.008.

Guy, H. P. (1977), Laboratory theory and methods for sediment analysis: Techniques of Water-Resources Investigation of the United States Geological Survey, Book 5, 58 pp.

Gyssels, G., J. Poesen, E. Bochet, and Y. Li (2005), Impact of plant roots on the resistance of soils to erosion by water: A review, *Prog. Phys. Geogr.*, *29*(2), 189–217, doi:10.1191/0309133305pp443ra.

Hairsine, P. B., and C. W. Rose (1992), Modeling water erosion due to overland flow using physical principles: 1. Sheet flow, *Water Resour. Res.*, *28*(1), 237–243, doi:10.1029/91WR02380.

Hart, S. C., T. H. DeLuca, G. S. Newman, M. D. MacKenzie, and S. I. Boyle (2005), Post-fire vegetative dynamics as drivers of microbial community structure and function in forest soils, *For. Ecol. Manage.*, *220*(1–3), 166–184, doi:10.1016/j.foreco.2005.08.012.

Heiri, O., A. F. Lotter, and G. Lemcke (2001), Loss on ignition as a method for estimating organic and carbonate content in sediments: Reproducibility and comparability of results, *J. Paleolimnol.*, *25*(1), 101–110, doi:10.1023/a:1008119611481.

Horton, R. (1945), Erosional development of streams and their drainage basins; hydrophysical approach to quantitative morphology, *Geol.Soc. Am. Bull.*, *56*(3), 275–370, doi:10.1130/0016-7606(1945)56[275:edosat]2.0.co;2.

Hungerford, R. D., M. G. Harrington, W. H. Frandsen, K. C. Ryan, and G. J. Niehoff (1991), Influence of fire on factors that affect site productivity, *Proc. Manage. Prod. Western-Montane Forest Soils*, *280*, 32–50.

Jenny, H. (1994), *Factors of Soil Formationa System of Quantitative Pedology*, McGraw-Hill, New York 1941.

Julien, P. Y. (1998), *Erosion and Sedimentation*, Cambridge Univ. Press, New York.

Kean, J. W., D. M. Staley, and S. H. Cannon (2011), In situ measurements of post-fire debris flows in southern California: Comparisons of the timing and magnitude of 24 debris-flow events with rainfall and soil moisture conditions, *J. Geophys. Res.*, *116*, F04019, doi:10.1029/2011JF002005.

Kemper, W. D., R. C. Rosenau, and A. R. Dexter (1987), Cohesion development in disrupted soils as affected by clay and organic matter content and temperature, *Soil Sci. Soc. Am. J.*, *51*(4), 860–867, doi:10.2136/sssaj1987.03615995005100040004x.

Kinner, D. A., and J. A. Moody (2008) Infiltration and runoff measurements on steep burned hillslopes using a rainfall simulator with variable rain intensities, U.S. Geological Survey Scientific Investigations Report 2007-5211. 64 p.

Knapen, A., J. Poesen, G. Govers, G. Gyssels, and J. Nachtergaele (2007), Resistance of soils to concentrated flow erosion: A review, *Earth Sci. Rev.*, *80*(1–2), 75–109, doi:10.1016/j.earscirev.2006.08.001.

Laflen, J. M., W. J. Elliot, D. C. Flanagan, C. R. Meyer, and M. A. Nearing (1997), WEPP-predicting water erosion using a process-based model. (computer model for predicting soil erosion), *J. SoilWatar Conserv.*, *52*(2), 96–102.

Lane, P., G. J. Sheridan, P. J. Noske, C. B. Sherwin, J. Costenaro, P. Nyman, and H. G. Smith (2011), Fire effects on forest hydrology: Lessons from a multi-scale catchment experiment in SE Australia, paper presented in Revisiting Experimental Catchment Studies in Forest Hydrology, Proceedings of a Workshop held during the XXV IUGG General Assembly, Melbourne, July 2011.

Larsen, I. J., J. L. Pederson, and J. C. Schmidt (2006), Geologic versus wildfire controls on hillslope processes and debris flow initiation in the Green River canyons of Dinosaur National Monument, *Geomorphology*, *81*(1-2), 114–127, doi:10.1016/j.geomorph.2006.04.002.

Léonard, J., and G. Richard (2004), Estimation of runoff critical shear stress for soil erosion from soil shear strength, *Catena*, *57*(3), 233–249, doi:10.1016/j.catena.2003.11.007.

Mataix-Solera, J., A. Cerdà, V. Arcenegui, A. Jordán, and L. M. Zavala (2011), Fire effects on soil aggregation: A review, *Earth Sci. Rev.*, *109*(1–2), 44–60, doi:10.1016/j.earscirev.2011.08.002.

McCoy, S. W., J. W. Kean, J. A. Coe, G. E. Tucker, D. M. Staley, and T. A. Wasklewicz (2012), Sediment entrainment by debris flows: In situ measurements from the headwaters of a steep catchment, *J. Geophys. Res.*, *117*, F03016, doi:10.1029/2011JF002278.

Megahan, W. F. (1974), Erosion over time on severely disturbed granitic soils a model, *Rep* INT-156, 1-20 pp, US Forest Service, Intermountain forest and range experiment station, Ogden, Utah.

Michaletz, S. T., and E. A. Johnson (2007), How forest fires kill trees: A review of the fundamental biophysical processes, *Scand. J. For. Res.*, *22*, 500–515, doi:10.1080/02827580701803544.

Moffet, C. A., F. B. Pierson, P. R. Robichaud, K. E. Spaeth, and S. P. Hardegree (2007), Modeling soil erosion on steep sagebrush rangeland before and after prescribed fire, *Catena*, *71*(2), 218–228, doi:10.1016/j.catena.2007.03.008.

Moody, J. A., and B. A. Ebel (2012), Hyper-dry conditions provide new insights into the cause of extreme floods after wildfire, *Catena*, *93*(0), 58–63, doi:10.1016/j.catena.2012.01.006.

Moody, J. A., and B. A. Ebel (2013), Infiltration and runoff generation processes in fire-affected soils, *Hydrol. Processes*, doi:10.1002/hyp.9857.

Moody, J. A., and P. Nyman (2013), Variations in soil detachment rates after wildfire as a function of soil depth, flow and root properties. Scientific investigations report, *Rep* 2012-5233., US Geological Survey, Virginia.

Moody, J. A., J. D. Smith, and B. W. Ragan (2005), Critical shear stress for erosion of cohesive soils subjected to temperatures typical of wildfires, *J. Geophys. Res.*, *110*, F01004, doi:10.1029/2004JF000141.

Moody, J. A., D. A. Martin, and S. H. Cannon (2008), Post-wildfire erosion response in two geologic terrains in the western USA, *Geomorphology*, *95*(3-4), 103–118, doi:10.1016/j.geomorph.2007.05.011| ISSN0169-555X.

Moody, J. A., R. A. Shakesby, P. R. Robichaud, S. H. Cannon, and D. A. Martin (2013), Current research issues related to post-wildfire runoff and erosion processes, *Earth Sci. Rev.*, *122*, 10–37, doi:10.1016/j.earscirev.2013.03.004.

Morgan, R. P. C., J. N. Quinton, R. E. Smith, G. Govers, J. W. A. Poesen, K. Auerswald, G. Chisci, D. Torri, and M. E. Styczen (1998), The European Soil Erosion Model (EUROSEM) a dynamic approach for predicting sediment transport from fields and small catchments, *Earth Surf. Processes Landforms*, *23*(6), 527–544, doi:10.1002/(sici)1096-9837(199806)23:6<527:aid-esp868>3.0.co;2-5.

Nachtergaele, J., and J. Poesen (2002), Spatial and temporal variations in resistance of loess-derived soils to ephemeral gully erosion, *Eur. J. Soil Sci.*, *53*(3), 449–463, doi:10.1046/j.1365-2389.2002.00443.x.

Nearing, M. A., G. R. Foster, L. J. Lane, and S. C. Finkner (1989), A process-based soil-erosion model for USDA water erosion prediction project technology, *Trans. ASAE*, *32*(5), 1587–1593.

Neary, D. G., C. C. Klopatek, L. F. DeBano, and P. F. Ffolliott (1999), Fire effects on belowground sustainability: A review and synthesis, *For.Ecol. Manage.*, *122*(1-2), 51–71, doi:10.1016/S0378-1127(99)00032-8.

Nyman, P., G. J. Sheridan, H. G. Smith, and P. N. J. Lane (2011), Evidence of debris flow occurrence after wildfire in upland catchments of south-east Australia, *Geomorphology*, *125*(3), 383–401, doi:10.1016/j.geomorph.2010.10.016.

Onda, Y., W. E. Dietrich, and F. Booker (2008), Evolution of overland flow after a severe forest fire, Point Reyes, California, *Catena*, *72*(1), 13–20, doi:10.1016/j.catena.2007.02.003.

Parsons, A. J., P. R. Robichaud, S. A. Lewis, C. Napper, and J. T. Clark (2010), *Field guide for mapping post-fire soil burn severity*, *Rep RMRS-GTR-243*, pp. 49, USDA, Rocky Mountain Research Station, Fort Collins, Colorado.

Prosser, I. P., and L. Williams (1998), The effect of wildfire on runoff and erosion in native Eucalyptus forest, *Hydrol. Processes*, *12*(2), 251–265, doi:10.1002/(SICI)1099-1085(199802)12:2<251::AID-HYP574>3.0.CO;2-4.

Rauws, G., and G. Covers (1988), Hydraulic and soil mechanical aspects of rill generation on agricultural soils, *J. Soil Sci.*, *39*(1), 111–124, doi:10.1111/j.1365-2389.1988.tb01199.x.

Rickenmann, D. (1991), Hyperconcentrated flow and sediment transport at steep slopes, *J. Hydraul. Eng.*, *117*(11), 1419–1439, doi:10.1061/(ASCE)0733-9429(1991)117:11(1419).

Robichaud, P. R., J. W. Wagenbrenner, and R. E. Brown (2010), Rill erosion in natural and disturbed forests: 1. Measurements, *Water Resour. Res.*, *46*, W10506, doi:10.1029/2009WR008314.

Schumm, S. (1956), Evolution of drainage systems and slopes and slopes in badlands at Perth Amboy, New Jersey, *Geol.Soc. Am.Bull.*, *67*(5), 597–646, doi:10.1130/0016-7606(1956)67[597:eodsas]2.0.co;2.

Sheridan, G. J., H. B. So, R. J. Loch, and C. M. Walker (2000), Estimation of erosion model erodibility parameters from media properties, *Soil Res.*, *38*(2), 265–284, doi:10.1071/SR99041.

Sheridan, G. J., P. N. J. Lane, and P. J. Noske (2007), Quantification of hillslope runoff and erosion processes before and after wildfire in a wet Eucalyptus forest, *J. Hydrol.*, *343*(1-2), 12–28, doi:10.1016/j.jhydrol.2007.06.005.

Sheridan, G. J., P. N. J. Lane, C. B. Sherwin, and P. J. Noske (2011), Post-fire changes in sediment rating curves in a wet Eucalyptus forest in SE Australia, *J. Hydrol.*, *409*(1–2), 183–195, doi:10.1016/j.jhydrol.2011.08.016.

Smirnova, E., Y. Bergeron, S. Brais, and A. Granström (2008), Postfire root distribution of Scots pine in relation to fire behaviour, *Can. J. For. Res.*, *38*, 353–362, doi:10.1139/X07-127.

Smith, H. G., G. J. Sheridan, P. N. J. Lane, P. J. Noske, and H. Heijnis (2011), Changes to sediment sources following wildfire in a forested upland catchment, southeastern Australia, *Hydrol. Processes*, *25*(18), 2878–2889, doi:10.1002/hyp.8050.

Smith, H. G., G. J. Sheridan, P. Nyman, D. P. Child, P. N. J. Lane, M. A. C. Hotchkis, and G. E. Jacobsen (2012), Quantifying sources of fine sediment supplied to post-fire debris flows using fallout radionuclide tracers, *Geomorphology*, *139–140*, 403–415, doi:10.1016/j.geomorph.2011.11.005.

Tennant, D. (1975), A test of a modified line intersect method of estimating root length, *J. Ecol.*, *63*(3), 995–1001.

Tisdall, J. M., and J. M. Oades (1982), Organic matter and water-stable aggregates in soils, *J. Soil Sci.*, *33*(2), 141–163.

Wagenbrenner, J. W., P. R. Robichaud, and W. J. Elliot (2010), Rill erosion in natural and disturbed forests: 2. Modeling approaches, *Water Resour. Res.*, *46*, W10507, doi:10.1029/2009WR008315.

Waldron, L., and S. Dakessian (1981), Soil reinforcement by roots: Calculation of increased soil shear resistance from root properties, *Soil Sci.*, *132*(6), 427–435.

Wells, G. (1987), The effects of fire on the generation of debris flows in southern California, *Rev.Eng. Geol.*, *7*, 105–114.

Whicker, J. J., J. E. I. I. I. Pinder, and D. D. Breshears (2006), Increased wind erosion from forest wildfire: Implications for contaminant-related risks, *J. Environ. Qual.*, *35*, 468–478, doi:10.2134/jeq2005.0112.

Wiberg, P. L., and J. D. Smith (1987), Calculations of the critical shear stress for motion of uniform and heterogeneous sediments, *Water Resour. Res.*, *23*(8), 1471–1480, doi:10.1029/WR023i008p01471.

Wilson, C. J. (1999), Effects of logging and fire on runoff and erosion on highly erodible granitic soils in Tasmania, *Water Resour. Res.*, *35*(11), 3531–3546, doi:10.1029/1999WR900181.

Wischmeier, W. H., and J. V. Mannering (1968), Relation of soil properties to its erodibility, *Soil Sci. Soc. Am. J.*, *33*(1), 131–137, doi:10.2136/sssaj1969.03615995003300010035x.

Wondzell, S. M., and J. G. King (2003), Postfire erosional processes in the Pacific Northwest and Rocky Mountain regions, *For. Ecol. Manage.*, *178*(1-2), 75–87, doi:10.1016/S0378-1127(03)00054-9.

Woods, S. W., and V. N. Balfour (2010), The effects of soil texture and ash thickness on the post-fire hydrological response from ash-covered soils, *J. Hydrol.*, *393*(3-4), 274–286, doi:10.1016/j.jhydrol.2010.08.025.

Zhang, X.-C., Z.-B. Li, and W.-F. Ding (2005), Validation of WEPP sediment feedback relationships using spatially distributed rill erosion data, *Soil Sci. Soc. Am. J.*, *69*(5), 1440–1447, doi:10.2136/sssaj2004.0309.

Zhang, G. H., Y. M. Liu, Y. F. Han, and X. C. Zhang (2009), Sediment transport and soil detachment on steep slopes: II. Sediment feedback relationship, *Soil Sci. Soc. Am. J.*, *73*(4), 1298–1304, doi:10.2136/sssaj2009.0074.

Ziegler, A. D., R. A. Sutherland, and T. W. Giambelluca (2000), Partitioning total erosion on unpaved roads into splash and hydraulic components: The roles of interstorm surface preparation and dynamic erodibility, *Water Resour. Res.*, *36*(9), 2787–2791, doi:10.1029/2000WR900137.

Zimbone, S. M., A. Vickers, R. P. C. Morgan, and P. Vella (1996), Field investigations of different techniques for measuring surface soil shear strength, *Soil Technol.*, *9*(1–2), 101–111, doi:10.1016/0933-3630(96)00002-5.